Open-Coast Tidal Flats

9

Daidu Fan

Abstract

Recent research advances highlight the importance of open-coast tidal-flat depositional system in both modern and ancient coastal environments. The system is unique in its wave- and tide-dominated physical setting, notably distinct from the tide-dominated barred tidal flats and the wave-dominated shorefaces. Interactions of waves and tides over different time scales produce not only cyclic morphologic variations in terms of erosion and deposition, but also rhythmic depositional units consisting of storm-generated sand-dominated layers (SDLs) and post-storm mud-dominated layers (MDLs). Ancient deposits of the open-coast tidal flats can be distinguished by abundance of storm-generated structures and scarcity of tidal-channel deposits from those of barred tidal flats, and by abundance of the structures created by combined flows or the interactions of waves and tides from those of (tidal) shorefaces. Difference is also remarkable between muddy and sandy open-coast tidal flats. Muddy open-coast tidal flats tend to develop along mega-river deltas and the adjacent chenier plains, have a general accretional convex-up profile with clear zonation, and produce aggradational fining-upward intertidal successions. Sandy open-coast tidal flats are common in the open-mouth estuaries of small rivers and the adjacent strand plains, usually develop an erosional concave-up profile with common presence of inner swash bars having the coarsest sediment near the high water, and produce coarsening-upward retrogradational successions. The vertical successions of sandy open-coast tidal flats generally contain more storm-generated beds volumetrically than those of muddy open-coast tidal flats. Notably, there are some accretional sandy open-coast tidal flats, lying in between the above two settings. A new spectrum of coastal morphodynamic settings is therefore proposed to change from the tide-dominated barred tidal flats, the wave-influenced and tide-dominated muddy open-coast tidal flats, the wave- and tide-dominated accretional sandy open-coast tidal flats, the wave-dominated erosional sandy open-coast tidal flats, to the wave-dominated tidal shorefaces.

9.1 Introduction

Tidal flats can be developed in numerous environments, like lagoons, embayments, estuaries, deltas, and coastal plains, ranging from sheltered environments to those

D. Fan (✉)
State Key Laboratory of Marine Geology, Tongji University, Shanghai 200092, China
e-mail: ddfan@tongji.edu.cn

R.A. Davis, Jr. and R.W. Dalrymple (eds.), *Principles of Tidal Sedimentology*,
DOI 10.1007/978-94-007-0123-6_9,

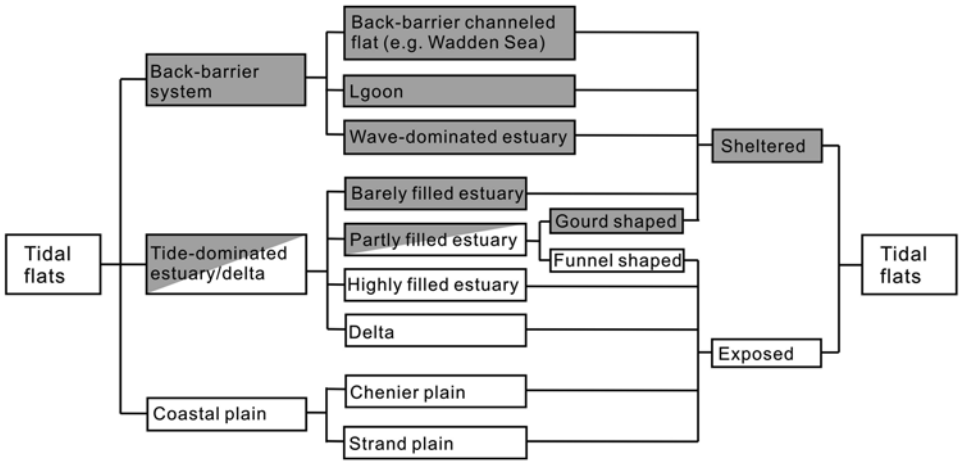

Fig. 9.1 Classifications of tidal flats and their relationships

completely exposed to the coastal sea or the open ocean (Fig. 9.1). Rudolf Richter, a German paleontologist, began the first systematic geologic studies of tidal flats along the German North Sea coast in the early 1920s. These studies were not only well carried on by his successors at the Senckenberg Institute but also rapidly spread out to the Netherlands, UK, and North America after the World War II (Ginsburg 1975; Middleton 1991; Klein 1998). Increased interest in fossil tidal deposits ignited comparative studies, and criteria for recognizing tidal-flat deposits were summarized: (1) cross-bedding with evidence for current reversals, like herringbone cross-stratification, reactivation surfaces, and mud couplets/drapes; (2) tidal bundles with evidence for tidal rhythms, e.g., diurnal, semilunar, and lunar cycles; (3) flaser and lenticular bedding in fining-upward successions (Middleton 1991; Nio and Yang 1991).

The well-known criteria for tidal-flat deposition obviously bear their regional background of the Wadden Sea and the Bay of Fundy (e.g., Klein 1985; Dalrymple 1992; Boggs 2005), that are classified as sheltered tidal flats (Fig. 9.1). The Wadden Sea is the tidal-channel-flat complex separating the barrier island system from the mainland, which in turn connects with the North Sea through the tidal inlets between each two barrier islands (Ginsburg 1975; Davis et al. 1998). In the Bay of Fundy, tidal flats occupy the innermost part of the estuary, separating the outer erosion zone with elongate sand bars (Dalrymple et al. 1991). The sheltered tidal flats are characterized by the presence of tidal sand bodies (linear shoals or bars) at the lower intertidal zone or the subtidal zone, and delicate tidal-channel systems cutting into the flats. Lateral migration of channel bars and/or high sedimentation rate in the sheltered settings are potential to produce rhythmic tidal-bundle successions or cyclic tidal rhythmites (Boersma and Terwindt 1981; Nio and Yang 1991; Dalrymple et al. 1991; Dalrymple 2010).

Over the past three decades, a deep passion has been intrigued toward finding tidalites with cyclic variations in bundle/lamina thickness, encoding tidal periodicities of neap-spring cycles, diurnal, fortnightly, and other longer inequalities (e.g., Boersma and Terwindt 1981; Kvale et al. 1989; Dalrymple et al. 1991; Tessier 1993; Williams 1997; Coughenour et al. 2009). The quantitative features (tidal periodicities) of the strata are significantly important in ascertaining their tidal origin, considering that most of qualitative features like flaser and lenticular bedding are not exclusive from non-tidal environments. The neap-spring periodicity of cyclic tidal rhythmites is also highly valued for reconstruction of the history of tides and lunar orbit throughout the geologic time from the Archean to the present (Coughenour et al. 2009). It is, however, noteworthy that the preservation of cyclic tidal rhythmites requires special conditions like sheltered areas with high sediment and accommodation-space availability

to achieve the continuous rapid deposition (Tessier 1993; Greb and Archer 1995; Fan and Li 2002; Fan et al. 2004a, b; Dalrymple 2010). Cyclic tidal rhythmites are therefore quite limited in their spatial and temporal distributions throughout the geological time (Davis et al. 1998).

Noncyclic tidalites are actually much more widely distributed than the cyclic tidal rhythmites, considering that most of tidal flats are not exclusive from wave impacts. The exposure to wave increases from tidal flats fringing open-mouth estuaries, deltas, to coastal plains, which are all referred as open-coast tidal flats in this context (Fig. 9.1). The recent studies highlight that the interaction of tides and waves is major mechanism for sediment transport and morphological and stratigraphic formation on open-coast tidal flats (Allen and Duffy 1998; Li et al. 2000; Fan et al. 2004a, b, 2006; Lee et al. 2004). Moreover, some sandy open-coast tidal flats can be wave dominated (Yang et al. 2005; Dalrymple et al. 2006). The strata of open-coast tidal flats are characterized by containing a mixture of tide- and wave-generated sedimentary structures with a general increase in the thickness ratio of storm deposition and tidal deposition as the wave exposure increases. It should therefore undoubtedly lead to misidentification of the open-coast tidal-flat deposition, if the pure tide-depositional criteria were employed for facies interpretation (Dalrymple 2010).

Open-coast tidal flats remained less studied until the current century, although they are much more widely distributed than the sheltered tidal flats along the world coast, and their importance for both modern and ancient tidal sedimentology has been highlighted since the mid-1970s (Klein 1975; Wang 1983; Ren 1985; Wells et al. 1990; Fan et al. 2004a; Yang et al. 2005). Several reasons account for the situation. Open-coast tidal flats are majorly composed of fine-grained sediment with mud domination, which is usually considered less economically important for resource exploitation. Muddy open-coast tidal flats are principally distributed along the coasts of South and East Asia, Oceania, and South America, receiving gigantic volume of fluvial fine sediment (Figs. 9.2–9.4), which are less accessible to Western European and North American. Although Chinese scientists began pilot studies of tidal flats in the early 1960s (e.g., Wang 1963; Li et al. 1965), most of their research results were published in Chinese (see a review given by Shi and Chen 1996), also unreadable to the western scientific community. Sandy exposed tidal flats are common along the open coast neighboring small river mouth, nourished by riverine sediment principally composed of coarse grains (coarse silt and sand), like the central west coast of Taiwan (Reineck and Cheng 1978), the southwest coast of Korea (Yang et al. 2005), the east and northwest coast of India (Mukherjee et al. 1987) and the northwest coast of Australia (Semeniuk 1981). They are also common in parts of Western Europe and North America, like the coast of the southwestern English Channel, the Irish Sea, and the Strait of Georgia in Canada (Hale and McCann 1982; Deloffre et al. 2007; Yang et al. 2008a). The sandy open-coast tidal flats lie at a transitional ground between the tide-dominated muddy open-coast tidal flats and wave-dominated shorefaces, and their affinity to wave dynamics and shoreface morphology makes them easy to be misinterpreted as tidal beach. All of these may account for their having been much less studied until the present decade (Yang et al. 2005, 2008a; Dalrymple 2010).

There has been a rapid increase in publications on open-coast tidal flats since the beginning of the new century. The topics cover all fields including hydrodynamics, sediment- and morphodynamics, sedimentology, and stratigraphy, especially those in China and Korea (Li et al. 2000, 2005a; Chang and Choi 2001; Fan 2001; Fan and Li 2002; Fan et al. 2001, 2002, 2004a, b, 2006; Kim 2003; Yang et al. 2005, 2006a, b, 2008a, b; Dalrymple et al. 2006; Gao 2009; Wang et al. 2009). In these studies, open-coast tidal flats have been highlighted as a major coastal setting, significantly different from the well-known sheltered tidal flats and tidal beaches. This chapter attempts to summarize these research progresses on open-coast tidal flats, cultivating a general sedimentary model for future comparison studies of the systems.

9.2 Depositional Systems

Tidal flats are low-relief environments typically flanking the coast of broad shelf with marked tidal rhythms (Fig. 9.2). Macrotidal conditions undoubtedly favor the development of extensive tidal flats, but they are also common in mesotidal to microtidal coasts (Eisma 1998). Sediment supply (source, flux, and size) and the magnitude of exposure to waves are two other key factors controlling tidal-flat morphology and sedimentology.

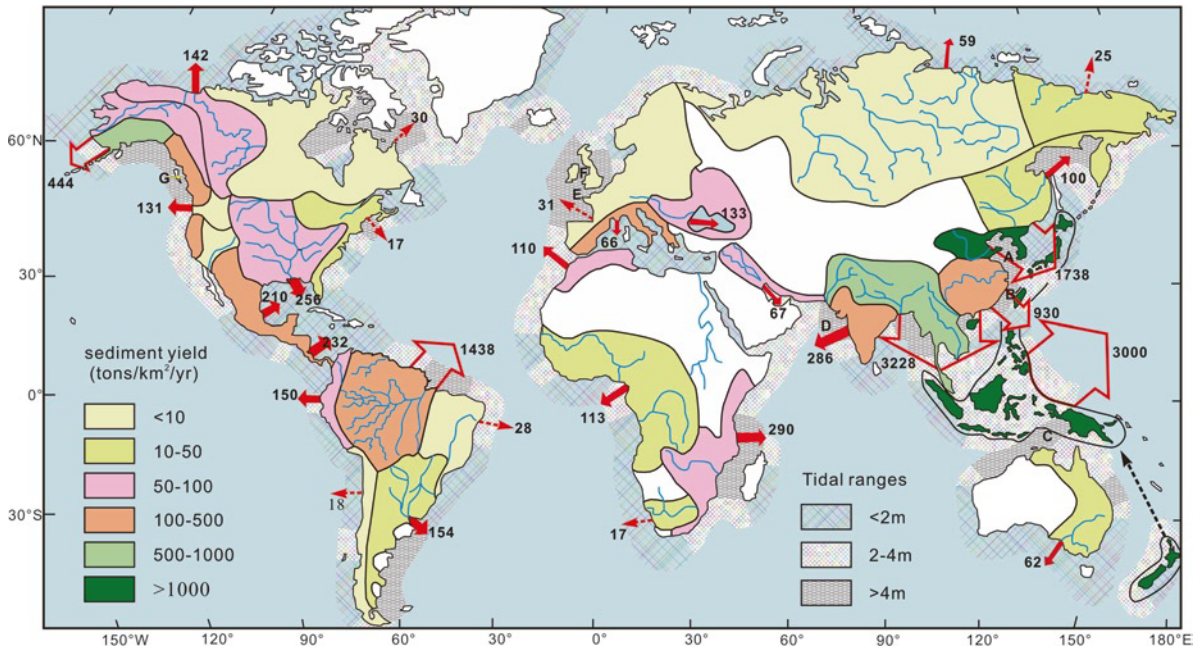

Fig. 9.2 Distribution of annual sediment discharge into the sea (millions of tons per year, modified after Milliman and Meade 1983; Milliman and Syvitski 1992) and spring tidal range (m) along the world's coasts (after Davies 1972). *A*: Yellow Sea, *B*: Taiwan Strait, *C*: Torres Strait, *D*: Arabian Sea, *E*: English Channel, *F*: Irish Sea, *G*: Strait of Georgia

Tidal flats are therefore classified into three major types: (1) back-barrier coast, (2) tide-dominated estuary/delta, and (3) coastal plain, with increasing wave exposure from low to high (Figs. 9.1 and 9.5).

Back-barrier tidal flats are referred to those occupying the landward side of barrier islands, spits, and bars, which serve as wave breakers (Fig. 9.5a, b). The back-barrier area can be partly occupied by tidal flats like those in lagoons and wave-dominated estuaries, or entirely filled with the tidal channel and flat system like the Wadden Sea. All of them receive limited sediment input from land. Back-barrier tidal flats typically develop extensively along the North Sea coast, and the Atlantic coast of Europe and North America (Flemming, Chap. 10 in this volume), which are both trailing edge coast receiving limited fluvial sediment input. They can also develop along the leading edge coast receiving abundant sediment like the Pacific US coast (e.g., Alaska and North California).

Tidal flats fringing the tide-dominated estuaries/deltas have varied magnitudes of wave exposure. Those are generally exempted from wave influence in the innermost part of the estuarine-deltaic system or in the estuaries having a guard (bottle-neck) shape (Fig. 9.5c). The outer part of the open-mouth estuaries and deltas are subject to wave impacts, especially during storm seasons (Fig. 9.5d–f). For example, wave influence is generally absent for the tidal flats in the inner part of the Xiangshan Bay deeply cutting into the land and Sanmeng Bay, while it gradually increases toward the baymouth. The straight coast of the highly filled Jiaojiang Estuary is completely open to the sea in the Zhejiang Province, central east of China (Fig. 9.6). In general, small river estuaries of tide domination usually foster sandy tidal flats because of limited fine sediment input from the rivers, except those receiving large volume of fine-grained sediment from the adjacent mega-river deltas by alongshore transport, like the estuaries along the Zhejiang coast nourished by Changjiang-sourced sediment (Figs. 9.3 and 9.6). Therefore, sandy estuarine and strand plain tidal flats are commonly distributed along the coast of islands or peninsulas enclosing a broad and shallow strait or epeiric sea, where fine-grained sediment is generally exempted and macrotide is highly favorable owing to the morphological amplification, like the Yellow Sea, the Taiwan Strait, the Torres Strait, the Arabian Sea, the English Channel, the Irish Sea, the Strait of Georgia, and so on (Fig. 9.2).

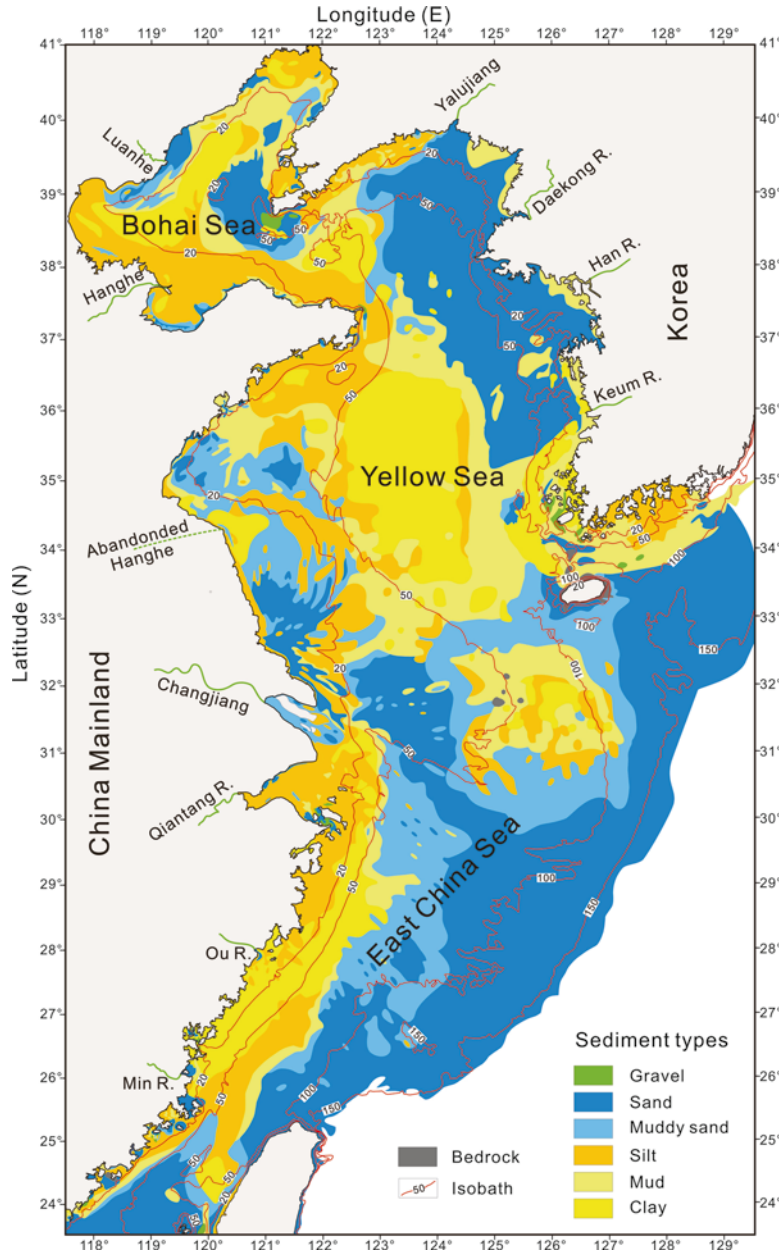

Fig. 9.3 Distribution of bottom sediment types and tidal flats that the coasts are surrounded directly by fine-grained deposits in light to dark yellow in the Bohai Sea, the Yellow Sea, and the East China Sea (After Li et al. 2005b)

Tidal flats flanking the coastal plains are directly open to the sea, thereby named as truly open-coast tidal flats (Dalrymple, pers comm 2010). Muddy and sandy open-coast tidal flats are generally linked to tide-dominated deltas/estuaries of large and small rivers, respectively. Larger river deltas tend to foster wider (cross-shore) and longer (alongshore) muddy tidal flats bordering the extensive chenier plains. Muddy open-coast tidal flats are globally widely extensive, considering that most of mega-river deltas are tide dominated or under significant tidal influence, building up extensive Holocene chenier plains in the world (Fig. 9.2, Table 9.1). The two longest stretches of muddy open-coast tidal flats are linked to the river deltas of the Changjiang and the Amazon, respectively. North Jiangsu tidal flats stretch over 600 km long between the abandoned Huanghe Delta and the Changjiang Delta at a macrotidal setting (Figs. 9.2 and 9.3, Wang et al. 2002). Guiana tidal flats extend over 1,600 km long from the Amazon River Delta to the

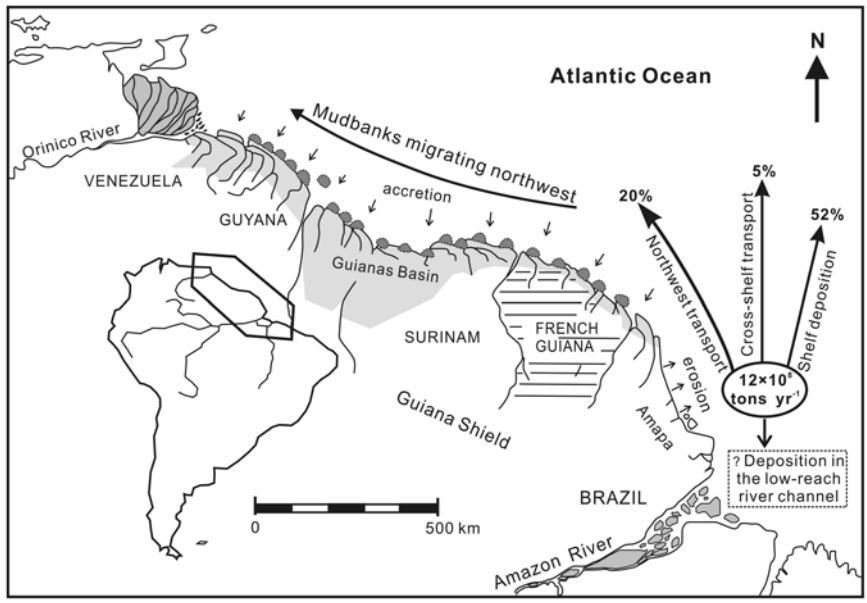

Fig. 9.4 Distribution of tidal flats (migrating mudbanks) along the coasts of northwest South America (Guiana) from the Amazon River mouth to the Orinoco River Delta (After Eisma et al. 1991; Plaziat and Augustinus 2004)

Orinoco River Delta (Fig. 9.4) at a macrotidal-to-mesotidal setting (Wells and Coleman 1981; Meade et al. 1985; Froidefond et al. 1988; Kineke et al. 1996; Baltzer et al. 2004). Sandy (truly) open-coast tidal flats are generally coexisting with sandy estuarine tidal flats (Fig. 9.2), bordering the Holocene strand plains of varied width (Reineck and Cheng 1978; Semeniuk 1981), or against the erosional Late Quaternary deposits or the rocky cliff (Thompson 1968; Semeniuk 1981; Yang et al. 2005).

Tidal flats are therefore classified into nine types in terms of coastal morphology (Figs. 9.1 and 9.5). They are in turn grouped into sheltered or exposed (open-coast) tidal flats on the basis of the magnitude of wave exposure. So the open-coast tidal flats in this context include both the truly open-coast tidal flats (i.e., coastal-plain tidal flats) and the partially sheltered to highly exposed tidal flats fringing the outer part of open-mouth estuaries and deltas (Fig. 9.1).

9.3 Physiography and Morphology

9.3.1 Tide, Wave, and Wind Climate

Strong tidal amplification occurs when tidal waves propagate into the broad and shallow shelf sea, consequently raising tidal range shoreward. The extreme case to induce tidal bores takes place when tidal waves enter a funnel-shaped embayment rapidly narrowing and shoaling landward (Archer and Hubbard 2003). The world's largest tidal bore occurs in the Hangzhou Bay, where the width of the bay decreases from ~100 km across the baymouth to <20 km along the Ganpu transection, while the mean tidal range increases landward from <2 m at the baymouth to over 5.5 m near Ganpu (Fig. 9.7). Epeiric seas and funnel-shaped bays were considered to be more prevalent in the geologic past, especially during the time of the supercontinent Pangea (Archer 1998), so macrotidal coastal settings should be common at that time.

Tidal currents are usually rotary on the open offshore area, gradually changing into linear when tides propagate into the distributary/estuarine channels or toward the shore. Main flows of flood and ebb tides in the estuaries and deltaic distributaries are steered toward different directions because of the Coriolis effect, resulting in different current strength and depositional patterns along the two different banks. In the Hangzhou Bay, flooding flows are steered north, and the convergent flows strengthen the current toward the north bank, producing the erosional and narrow tidal flats, while ebbing flows are steered south, and divergent and weakening flows favor developing the depo-

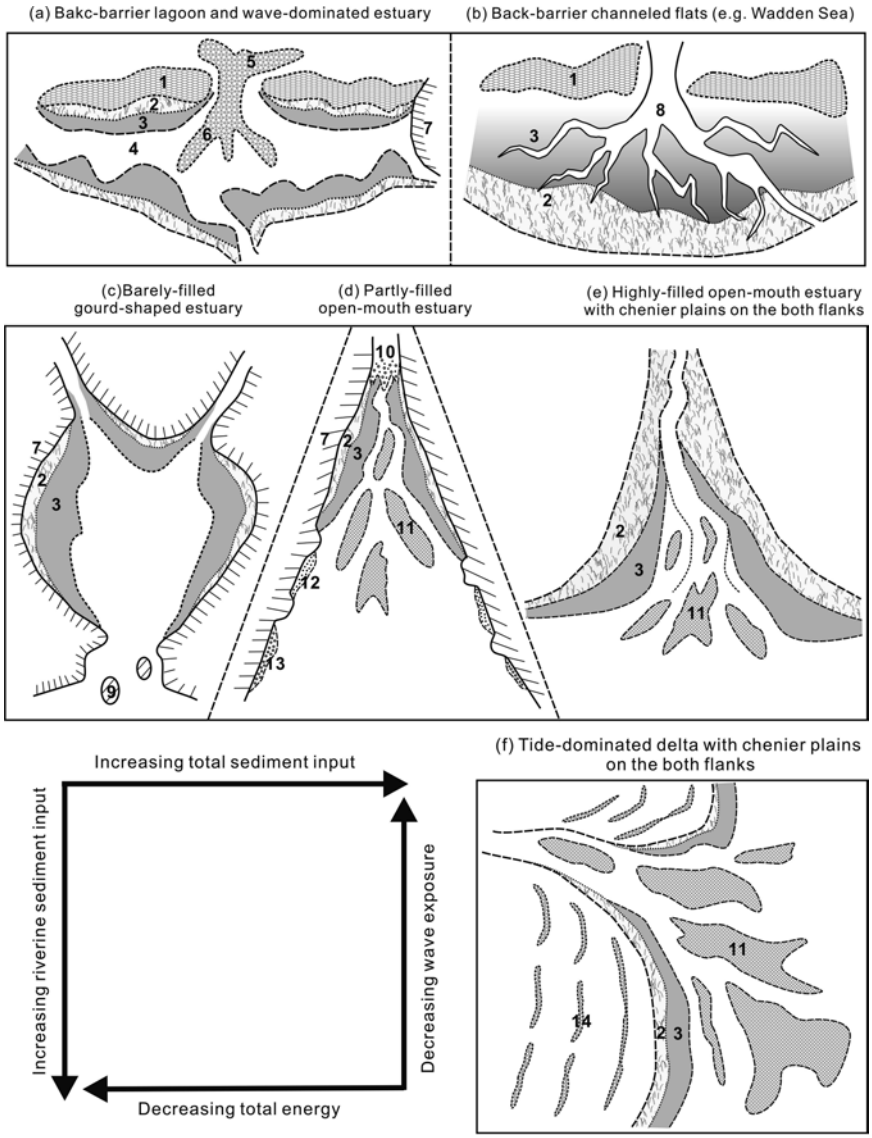

Fig. 9.5 Thematic plots of tidal flats in the different coastal systems with varying sediment input and wave exposure (**a**–**f**). *1* – barrier island, *2* – salt marsh, *3* – bare intertidal flat, *4* – lagoon, *5* – ebb tidal delta, *6* – flood tidal delta, *7* – rocky coast, *8* – tidal channel/creek, *9* – rocky island, *10* – bay-head delta, *11* – tidal sand ridge/bar, *12* – sand beach, *13* – gravel beach, *14* – chenier ridge

sitional and wide tidal flats along the south bank (Fig. 9.7; ECCE 1992; Fan et al. 2005). Constrained flows in the main channels of estuaries and deltaic distributaries are usually shore-parallel and ebb dominated, gradually changing into shore-normal direction and flood domination as they flow over the intertidal flats. Shore-normal tidal flow is generally quite weak due to limited tidal prism over the intertidal flats. The velocities of flood flows decrease from the subtidal zone to the upper intertidal flat owing to the shoaling effect. For example, the spring flood flow velocities decreased from 0.86 cm/s at a subtidal station (−2 m, elevation referred to Wusong Datum), 0.49 cm/s at 0 m, to 0.35 cm/s at an intertidal station (+2 m) on the Nanhui Mudbank in the Changjiang Delta (Li 1990).

The open-coast tidal flats are highly exposed to wave impact, and they are potential to change from the tide-dominated setting temporally (a few hours to days) or seasonally into the wave-dominated setting, especially where they are highly affected by the

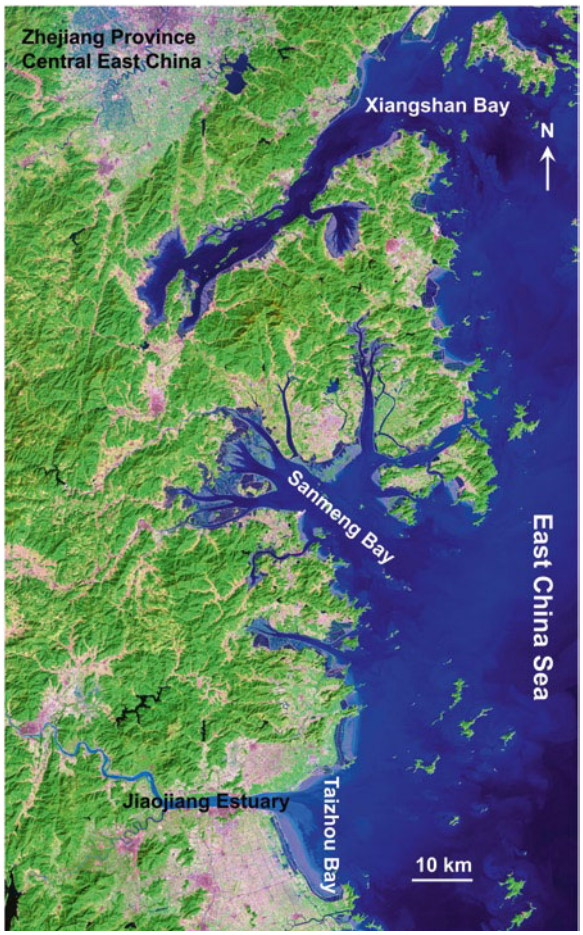

Fig. 9.6 Satellite photo of central-east Zhejiang coast showing the development of different tidal flats in the estuaries or embayments: (**a**) Xiangshan Bay, partly filled type with narrow baymouth and "¬" shape; (**b**) Sanmeng Bay, partly filled type with relatively narrow baymouth and gourd shape; (**c**) Jiaojiang Estuary-Taizhou Bay, highly filled coastal plain type with a wide baymouth and straight coastline Ð They are typical representative for the three major estuarine tidal flats in the classification lists of the Fig. 9.1

monsoon climate (Harris et al. 1993; Li et al. 2000; Yang et al. 2005; Fan et al. 2006). During the longer calm-weather season, shallow-water waves can be greatly attenuated when propagating over the gentle and broad subtidal zone, and the attenuated waves finally die out without breaking over the intertidal flats, especially where present with fluid mud (Wells and Coleman 1981; Lee et al. 1997; Kim 2003; Fan et al. 2006). Open-coast tidal flats can therefore be assigned as a tide-dominated or mix-energy tide-dominated coastal setting on the basis of Davis and Hayes' (1984) model (Fig. 9.8). While entering the storm season, rough seas generated by single events of tropical storms or winter cold fronts commonly sustain a few hours to days. They may also continue for a few weeks when more than two storms occur one after another. The open-coast tidal flats are consequently shifted into a mixed-energy wave-dominated or wave-dominated coastal setting for a few hours to weeks during the storms (Fig. 9.8). For example, the mean wave height on the Baeksu coast (SW Korea) is 0.5–1.0 m in summer, drastically elevated to 2–3 m in winter (Kim 2003; Yang et al. 2005), accounting for the development of typical depositional pattern "summer tidal flat – winter shoreface" (in the paper title of Yang et al. 2005).

In short, the open-coast tidal flats are generally characterized by large tidal range, weak shore-normal tidal flow, and high exposure to waves. These typical physical dynamics are conceived to develop the unique sedimentology and morphology of the open-coast tidal flats.

9.3.2 Landforms and Zonation

Tidal flats in this context are not limited to the intertidal zone, but also include supratidal and subtidal zones. The zonation can be generally defined: (1) by grain size into muddy, mixed, and sandy flats; (2) by vegetation into bare and vegetated flats; and (3) by tidal level into supratidal, intertidal, and subtidal flats. The intertidal flats can be further divided into upper, middle, and lower subdivisions (Fig. 9.9). However, the zonation boundary is quite varied among the different criteria of grain size, vegetation, and tidal level, and a worldwide zonation can only be distinguished by tidal levels (Amos 1995; Eisma 1998). Here we describe the zonation of tidal flats in a synthetical way instead of using single criteria, also considering the difference between muddy and sandy open-coast tidal flats.

The supratidal and the upper parts of intertidal flats are usually covered with vegetation, characterized by extraordinarily gentle relief, fine-grained deposits principally consisting of clay and fine silt, and higher concentration of organic matter. The canopies can be salt-marsh plants in the temperate zone like the Jiangsu and Zhejiang coast in China (Ren 1985; Wang and Eisma 1988, 1990; Fan et al. 2004a), and mangroves in the tropical zone like the Guiana coast (Fig. 9.10; Plaziat and Augustinus 2004), the northwest Australia coast (Semeniuk 1981), and the coast of the Gulf of Papua (Allison and Lee 2004; Walsh and Nittrouer 2004).

Table 9.1 Delta class for the 16 largest rivers with annual sediment load larger than 100 million tons (based on data of Milliman and Syvitski 1992)

Rank	River	Country	Sediment load (million tons/year)	Spring tidal range (m)	Delta class
1	Amazon	Brazil	1,200	4.9	T
2	Huanghe (Yellow)	China	1,100	1.13	R to R/W
3	Ganges-Brahmaputra	Bangladesh	1,060	3.63	T
4	Changjiang (Yangtze)	China	480	3.66	T
5	Mississippi	USA	400(210)[a]	0.43 (M)	R to R/W
6	Irrawaddy	Burma	260	2.71	T
7	Indus	Pakistan	250(59)[a]	2.62	T/W
8	Magdalena	Colombia	220	1.1	R/W
9	Godavari	India	170	1.2	W
10	Mekong	Vietnam	160	3.2	T/W
11	Orinoco	Venezuela	150	1.77	W/R/T
12	Song Hong (Red)	Vietnam	130	3.2	T-W
13	Narmada	India	125	9.0 (Max)	T
14	Colorado	USA	120(0.1)[a]	8.0 (Max)	T
15	Nile	Egypt	120(0)[a]	0.43	W
16	Fly	PNG	115	3.8	T

[a]400(210): sediment load before and after river damming
M mean tidal range, *Max* maximum tidal range, *R* river-dominated, *T* tide-dominated, *W* wave-dominated, *T-W* subequal wave and tidal domination, *R/W* river-dominated and wave-modified, *PNG* Papua New Guinea

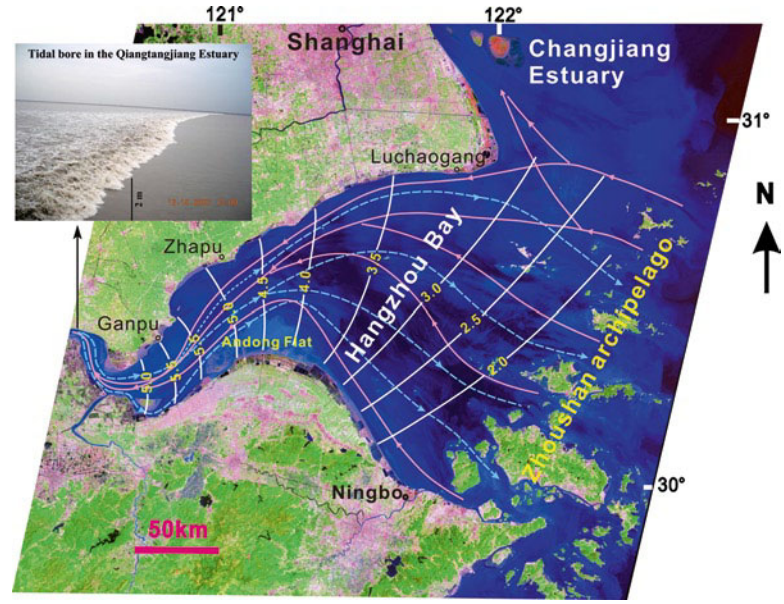

Fig. 9.7 Distribution patterns of mean tidal range, major tidal flow tracts in the Qiangtangjiang Estuary-Hangzhou Bay

In some dry regions, the higher part of tidal flats support only scant vegetation where salt pans can be well developed with sediment having higher concentration of evaporate minerals, like the Colorado Delta in the Northern Gulf of California (Thompson 1968, 1975; Meckel 1975). The vegetated flats usually grade landward into deltaic/chenier plains with little relief, which range from a few 100 m to over tens of kilometers in width, depending on the sediment supply. For example, the Holocene North Jiangsu coastal plain is more than

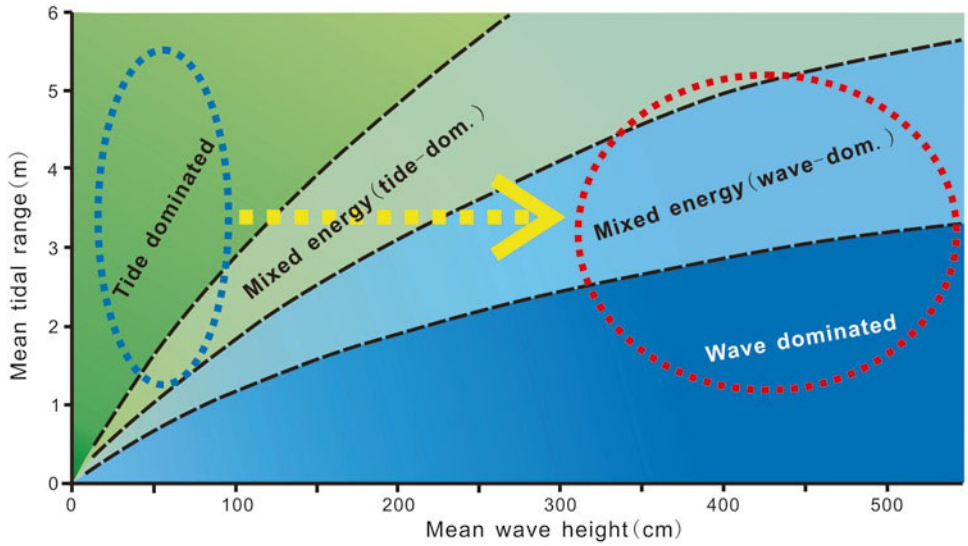

Fig. 9.8 Open-coast tidal flats shifting temporally from tide-dominated or mix-energy (tide-dom.) to wave-dominated regimes for a few days to weeks during summer/winter storms (Adapted from Davis and Hayes 1984)

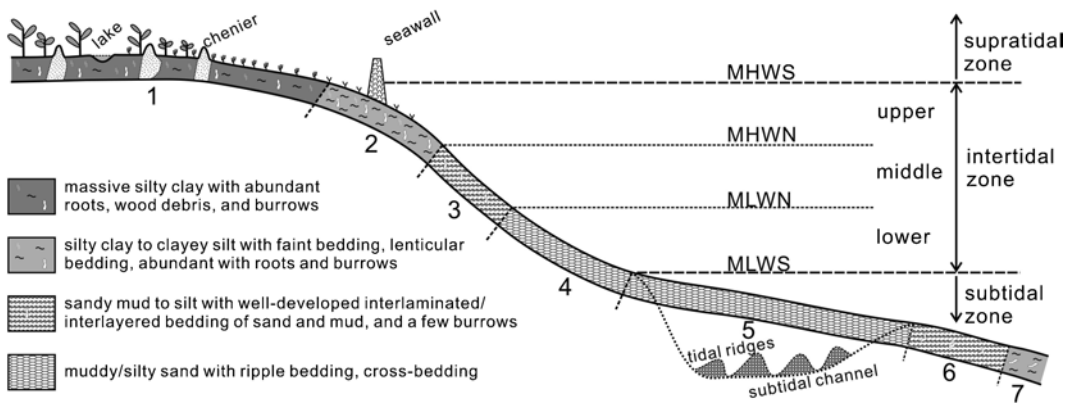

Fig. 9.9 Schematic map showing the cross-profile variations of tidal-flat morphology and sedimentology from the supratidal flats to the subtidal zones

60 km wide on average (Figs. 9.11 and 9.13), and the Holocene Guiana coastal plain ranges from 10 to 100 km wide with an average of ~30 km (Figs. 9.4 and 9.14, Rine and Ginsburg 1985; Allison et al. 1995a). In some sediment-starved coasts, the supratidal flats are narrow or even absent, bordering directly on the rocky hills like those along the Korean coast (Alexander et al. 1991; Yang et al. 2005).

The transition from the vegetated to the bare flats can be smooth or drastic with erosional cliff or channels. The mangrove land is usually surrounded by deeply cut tidal channels or cliffs (Semeniuk 1981; Plaziat and Augustinus 2004). A smooth transition generally occurs ahead of the accretional salt marshes, while recessional salt marshes tend to have an erosional escarpment at the front. Swash bars can be developed at the salt-marsh front on both accretional and recessional flats, resulting from wave breaking when storm waves ride on the high tides. On the Chongming Eastern Flat (Changjiang Delta), an accretional and smoothly transitional profile is favorable during weak-wave conditions (Fig. 9.12a), while it is replaced by the presence of erosional escarpment, scouring ponds, and swash sand sheets/bars consisting of coarse

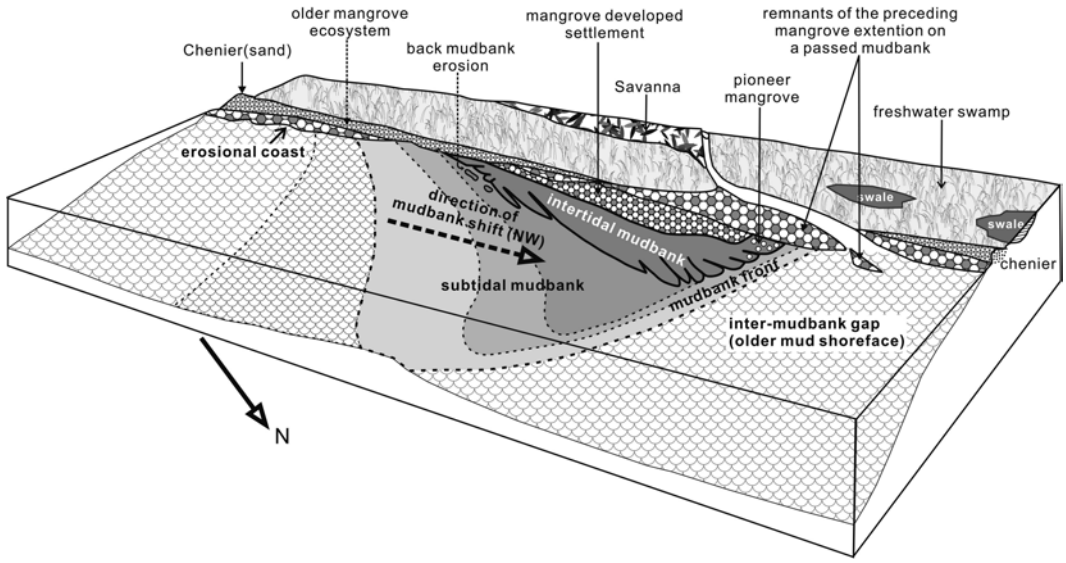

Fig. 9.10 Block diagram showing the zonations (including mangrove) and the shape of a shifting mudbank along the coast of Guianas (After Plaziat and Augustinus 2004). The intertidal area of the largest mudbanks is about 20–40 km long (alongshore) and 2–5 km wide

sediment and abundant shell debris during storm climates (Fig. 9.12b–f). Swash bars are conceivably the embryo of chenier ridges, which potentially develop into full chenier ridges if the processes continue for a longer term (over tens of to hundreds of years). Older chenier ridges are typically common on the extensive Holocene coastal plains abutting mega-river deltas, conceivably resulting from the long-term alternations of erosion (producing chenier) and accretion (depositing mud) linked to the secular fluctuation of river sediment discharge or shifting of the river main channel (Figs. 9.13 and 9.14, Rine and Ginsburg 1985; Liu and Walker 1989; Wang and Ke 1989; Eisma 1998).

Across the bare intertidal and subtidal flats, muddy and sandy open-coast tidal flats tend to have different cross-shore profiles and sediment distribution patterns. Muddy open-coast tidal flats usually have an accretional, convex-up cross-shore profile. The transition between the intertidal and the subtidal flats is generally smooth without a discernible relief, except those drop into the estuarine or deltaic-distributary channels with a higher slope (e.g., Ren 1985; Wang and Eisma 1988, 1990; Frey et al. 1989; Wang and Ke 1997; Fan et al. 2004a; Plaziat and Augustinus 2004, Figs. 9.9–9.11). Sediment on the accretional flats tends to be coarsest near the mean lower water springs, gradually fining landward and seaward from there. The intertidal zonations are roughly displayed with the lower sandy flat, the middle mixed (sand-mud) flat, and the upper muddy flat (Table 9.3). The zonation pattern was clearly shown by the surficial sediment distribution on the North Jiangsu tidal flats, typically along the rapid depositional section from Sheyang to Dafeng (Fig. 9.11; Wang and Ke 1997). On the central west coast of Korea where the estuarine/embayment tidal flats are well developed with mediate to high wave exposure, surficial sediment generally coarsens from fine silt/clay at the upper intertidal flats to coarse silt/fine sand at the lower intertidal flats (Frey et al. 1989; Alexander et al. 1991). It is noteworthy that the Guiana muddy tidal flats have the finest deposition mainly composed of silty clay (Table 9.3), showing little trend variations in grain size across the entire mudbank from the intertidal to the subtidal zones (Fig. 9.10, Rine and Ginsburg 1985; Allison et al. 1995a, b; Lefebvre et al. 2004).

Sandy open-coast tidal flats tend to have a concave-up cross-shore profile, commonly with very low (<1–2 mm year^{-1}) or even negative sedimentation rates (Semeniuk 1981; Hale and McCann 1982; Yang et al. 2005). The sandy lower intertidal flat is ordinarily very gentle and broad, but the seaward end is commonly bordered by ridge and runnel systems with significant undulations. The ridges are commonly shore-parallel with the crest-to-trough height of several decimeters to

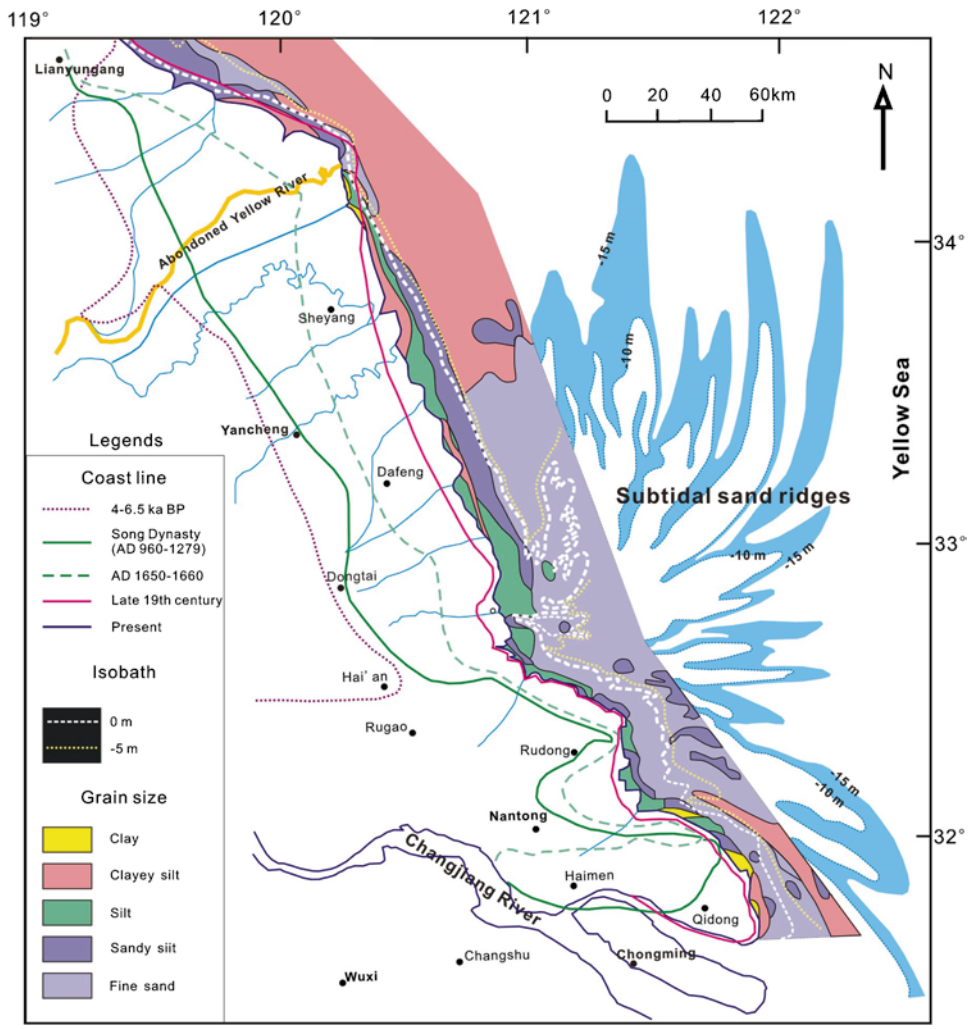

Fig. 9.11 Sediment distribution pattern for the extant tidal flats rimming the extensive Holocene coastal (chenier) plain of Jiangsu Province, China (After Wang and Ke 1997)

2–3 m, which are conceived to be generated like swash bars/ridges on the beach (Reineck and Cheng 1978; Yang et al. 2005). The sandy lower intertidal flat is landward continuous either with a gentle sand-mud middle intertidal flat and a mud upper intertidal flat for the accretional open coast like that on the central west coast of Taiwan (Reineck and Cheng 1978), or with a narrow inner slope like that on the coast of the Parksville Bay in the Strait of Georgia, Canada (Hale and McCann 1982), or with the inner swash bar/ridge and the inner muddy flat behind the bar/ridge like that on the southwest coast of Korea. The inner swash bar/ridge can be initially formed at the middle intertidal ground, migrates landward intermittently driven by seasonal storm events, and is finally welded to the coast as a part of the strand plain (Lee et al. 1994; Yang et al. 2005, 2008a; Ryu et al. 2008). The intertidal surficial sediment distribution has generally a landward-fining trend for the sandy open-coast intertidal flats without inner swash bar, similar to that of muddy open-coast tidal flats. However, a reverse trend, i.e., a landward-coarsening tendency except the inner muddy flat, is founded for those developing the inner swash bar composed of the coarsest sediment, which is highly mimic to the shoreface (Yang et al. 2005).

Tidal-channel networks are generally not much developed or event absent on the open-coast tidal flats in comparison with their delicate development on the

Fig. 9.12 Photos showing different morphologic and sedimentary features at the transitional zone between the salt marsh and the bare flats: (**a**) a gradual transition profile with soft muddy deposits on the flats, denoting accretion; (**b**) the erosion cliff of several centimeters high at the front of the salt marsh; (**c**) small erosion ponds on the salt-marsh land; (**d**) erosion remnant patches of partly consolidated salt-marsh deposits; (**e**) abundance of mud pebbles and shell debris on the erosion remnant patches; (**f**) swash sand sheet over the salt-marsh land

barred tidal flats (Frey et al. 1989; Wells et al. 1990; Alexander et al. 1991; Fan et al. 2004a; Yang et al. 2005). This is typically true for non-estuarine open-coast tidal flats, where the flats are exposed directly to the open sea. In the open-mouth estuaries, the main channels usually run parallel or oblique to local shoreline, but their landward branches are highly potential to cut deeply into the tidal flats, typically for those in the inner, less-exposed part of the estuaries. Although tidal channels are less developed on the bare flats, the broad vegetated flats tend to have tidal-creek networks as intricate as those on the sheltered tidal flats (Ren 1985;

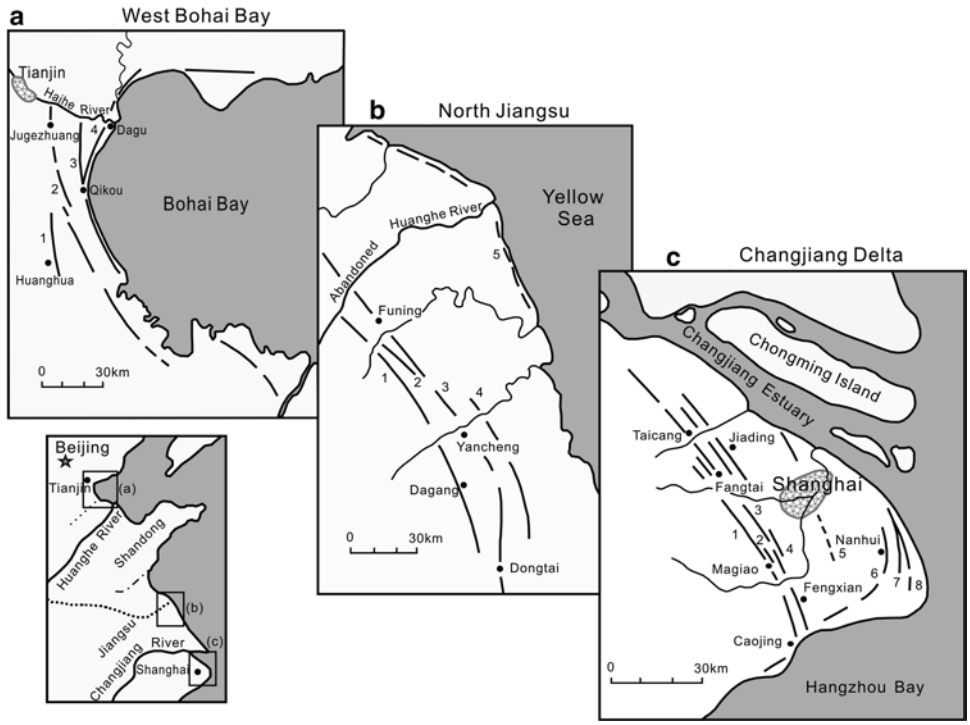

Fig. 9.13 The distribution of the chenier-ridge series on the coastal plain in East China (After Liu and Walker 1989)

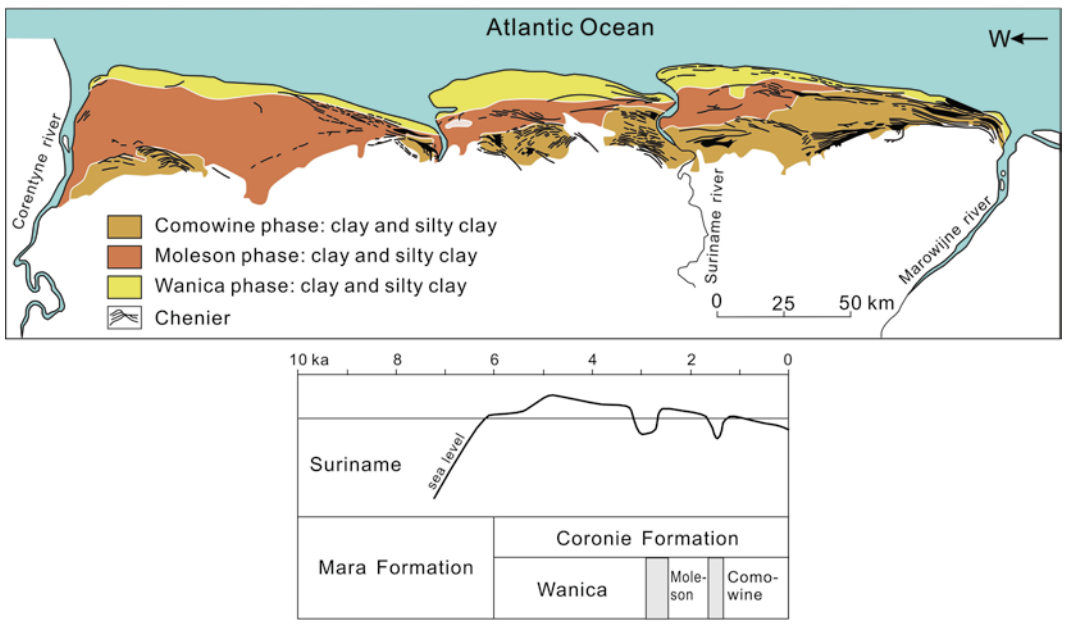

Fig. 9.14 Sketch map of the Surinam coastal plain showing the three-phase sedimentation units, separated by extensive chenier-bundle series denoting erosion phases (*upper panel*), and the relationship of regional sea-level fluctuations with alternations of accretion and non-deposition (erosion) phases during the Coronie Formation (*lower panel*, after Augustinus 2004)

Froidefond et al. 1988; Wang and Eisma 1988; Frey et al. 1989; Wells et al. 1990; Alexander et al. 1991; Zhang and Wang 1991; Eisma 1998; Fan et al. 2004a). On the Chongming Eastern Flats, the extensive salt-marsh land accommodates more than 20 tidal-creek dendritic networks (Fig. 9.15a). The larger the drainage basin, the more complicate the creek network. Small creeks usually terminate near the salt-marsh front, because the stability of creek banks decreases without protection by the vegetation and the slowing weak flows lose power to encroach the flats as the channel width increases toward the bare flats (Fig. 9.15b). Only a few large creeks continue their course on the bare flats from the marshland to the sea (Fig. 9.15a). The bare-flat channels are commonly shallow, muddy, and intermittent. They are potentially widened by big waves typically during storm or/and increasing flows during spring tides or heavy raining days (Fig. 9.15c–e), while they can be silted during small tides and waves. The tidal creek/channel system is therefore mainly functioned as a drainage network collecting and funneling water back to the sea during ebb tide, and flood current is less constrained by the shallow channels. Fine sediment dominates the creek/channel floor with frequent presence of fluid mud draining from the adjacent flats after exposure (Fan et al. 2004a).

In general, muddy and sandy open-coast tidal flats tend to have an accretional, convex-up and recessional, concave-up profile, respectively, which has been considered to be common morphodynamic features of tidal flats (Kirby 2000). The smoothed open-coast tidal flats are less dissected by tidal channels, conceivably linked to rotary current pattern, weak shore-normal component, and strong wave action. The most obvious relief over the entire tidal flats is the presence of inner and outer swash bars/ridges near the mean higher and lower water level, produced by storm waves during high tides and low tides, respectively. They are permanent or mobile, migrating landward intermittently driven by storm waves. The zonation pattern of intertidal sediment distribution is marked on the muddy open-coast tidal flats with a fining-landward trend, while it becomes blurry toward the sandy open-coast tidal flats. The latter potentially resembles the tidal beach in terms of a general coarsening-landward tendency and well-developed swash bars/ridges, occupying a transitional position between muddy open-coast tidal flats and tidal beach (Yang et al. 2008a; Dalrymple 2010).

9.4 Morphodynamics and Sediment Dynamics

9.4.1 Erosion and Deposition Cycles

The primary forces shaping intertidal flats are tidal currents and wind-induced waves. Waves are considered to be important for sediment suspension and currents for sediment advection. The interactions of waves and tides determine the magnitude and direction of sediment flux, and the resulting erosion and deposition are significantly site-specific over a small temporal scale ranging from a few minutes (wave frequency) to a few days (periods for intense waves/swells by meteorological events like tropical and subtropical storms). Intermediate erosion/deposition erosion cycles are mainly related to neap-spring cycles and seasonal alternations of wind and wave climate. Longer-term (decades to millennia) cycles of erosion and deposition are envisioned to take place over a larger spatial scale like the entire coastline of single deltas/estuaries or coastal basins. The super cycles are conceivably linked to longer-term variations in sediment supply (basin climate controlling), delta-lobe switching or the main channel shifting from one distributary to another, secular variations in sea-level change, and long-term sea wave climate change.

The short-term natural behavior of tidal flats can be monitored directly through the bed-level measurements or deduced indirectly through high-frequency measurements of waves, currents, and suspended sediment concentrations (SSC) during tidal inundation (Green et al. 1997; O'Brien et al. 2000; Lee et al. 2004; Thomas and Ridd 2004; Talke and Stacey 2008). Bed-level measurements are generally made during tidal exposure through using graduated stakes/poles, sediment erosion table (SET), and buried accretion plates, and sampling intervals usually vary from a single tidal cycle to 1 month (O'Brien et al. 2000; Thomas and Ridd 2004; Fan et al. 2006). Recent technical advances make it possible to monitor bed-level changes continuously during tidal inundation by employing acoustic transducer or submarine video camera (Christie et al. 1999; O'Brien et al. 2000; Thomas and Ridd 2004; Deloffre et al. 2007). Longer-term erosion/deposition cycles can be studied by the collection and comparison of the different-age satellite/aero photos or historical maps/charts. Dated sedimentary cores and chenier-ridge series are useful evidence for centennial to millennial cycles.

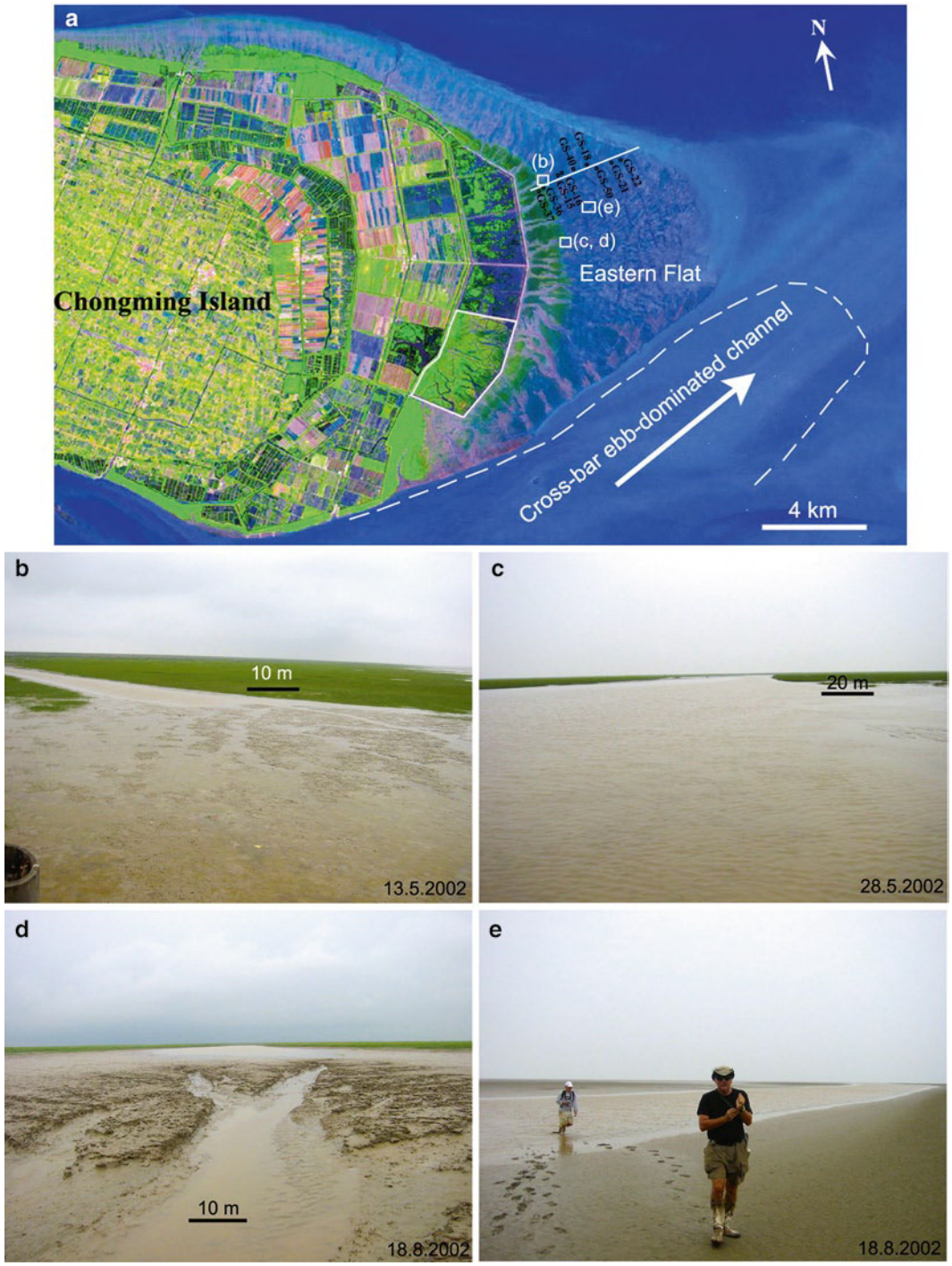

Fig. 9.15 (**a**) A satellite photo showing tidal creek/channel networks on the Chongming Eastern Flat in the Changjiang Delta, and the locations of the photos (**b**–**e**) taken and the elevation-monitoring stakes. (**b**) A tidal creek terminated near the boundary of the vegetated and bare flats. (**c**) A tidal creek continuing its course on the bare flat to the sea during spring tides or heavy raining days; (**d**) the shoal blocking the marsh creek dissected by head erosion due to increased creek discharge during spring tides with heavy raining. (**e**) A channel on the bare flat being widened by storm waves

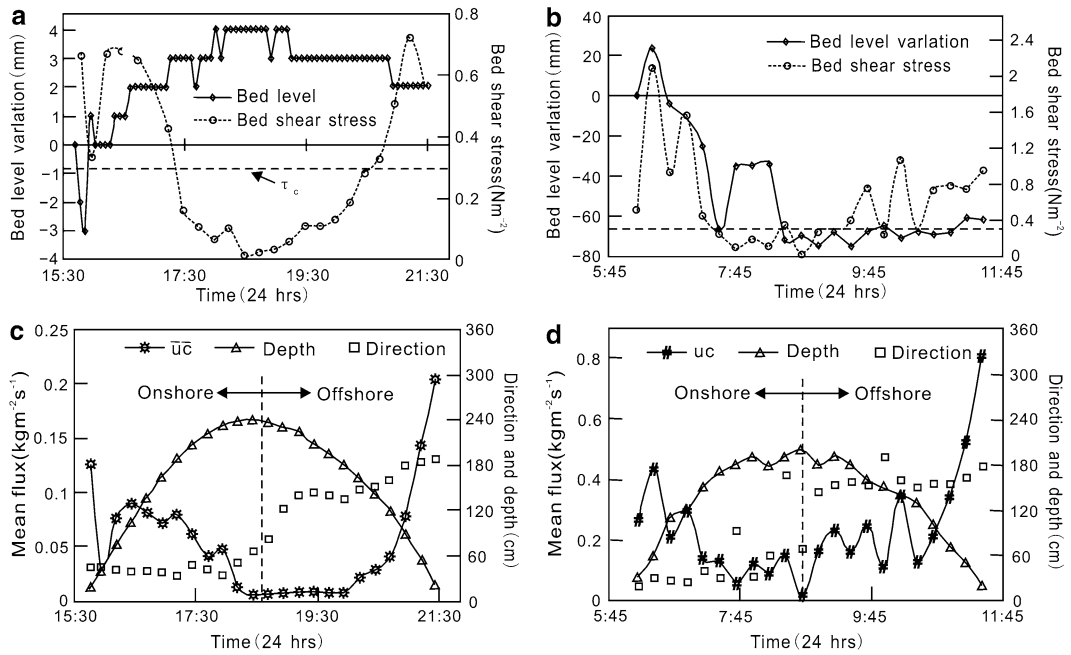

Fig. 9.16 Variation in hydrodynamic and morphodynamic processes within a tidal cycle on the Skeffling intertidal flat (Humber Estuary, UK) during the calm (**a** and **c**) and stormy (**b** and **d**) conditions. τ_c, the critical shear stress of sediment, was set to 0.3 N m^{-2}. Erosion occurs when $\tau_b > \tau_c$ (After Christie et al. 1999)

9.4.1.1 Short-Term Cycles (A Few Minutes to Days)

The interactions of tides and waves over a tidal cycle are fundamental processes and mechanisms to induce deposition and erosion on the open-coast tidal flats. Bottom shear stress is the important parameter to assess the deposition and erosion of sediments (e.g., Christie et al. 1999; Le Hir et al. 2000). Over the intertidal flats, purely tide-induced stresses are generally low to trigger significant erosion, while wave-induced stresses are much higher due to their orbital movement character. It has been widely acknowledged that even presence of small waves potentially enhances erosion of the surficial sediment significantly (Anderson et al. 1981; Christie et al. 1999; Le Hir et al. 2000; Lee et al. 2004). Enhanced erosion by large waves was nicely described by a comparison study of Christie et al. (1999) on a semi-closed and mega-tidal mudflat in the Humber Estuary (UK) with the average tidal range of ~6 m. The bed shear stresses (τ_b) of combined flows and waves were highly elevated toward the large-wave condition, producing several centimeters of erosion, which is strongly contrastive with a few millimeters of accretion during the small-wave condition (Fig. 9.16a, b).

The difference is highly outstanding between wave and tide processes over a tidal cycle. Tidal currents and tide-induced bottom stresses decrease landward from the lower intertidal flats, and drop to nearly zero at the high, slack tide. However, waves and wave-induced bottom stresses are significantly strengthened by the increased water depth during the rising tide owing to the relationship between wave height and water depth (Green et al. 1997; Le Hir et al. 2000).

So peak waves and the related processes hypothetically attain at high tide for any given location at the intertidal flats, and the slack (quiet) condition is consequently detained at high tide by the presence of large waves (Christie et al. 1999). The phenomena were clearly shown by the variations in $\overline{uc}$ value (mean suspended sediment flux, the product of mean current velocity and mean concentration of suspended sediment). The curve was flat with roughly zero value over approximately 1.5 h at high tide during small-wave condition (Fig. 9.16c), but was drastically replaced by a seesaw curve section during large-wave condition (Fig. 9.16d, Christie et al. 1999).

The shallow wave-break/swash zone should shift several 100–1,000 m landward and seaward over a

tidal cycle under the storm climate, violently disturbing the intertidal morphology over a wider area (Mao 1987; Shi and Chen 1996; Fan et al. 2006). The wave-break zone tends to stall respectively at low and high water line for longer time, hypothetically accounting for the development of inner and outer swash ridges as discussed in the former section.

Episodic high-energy events occur infrequently, but are the fiercest force to produce marked erosion and deposition cycles on the tidal flats. A large wave or storm event usually lasts several hours to days, so the resulted tidal-flat erosion and deposition pattern should be revealed only by a finer time scale than the life cycle of the events. Considering the complex interactions of waves and tides and a philosophy that a finer time scale tends to have a smaller spatial attribute, the episodically induced erosion/deposition phenomena should therefore be examined over a finer spatial scale. Following this, an experiment was carried out along a cross-profile on the Nanhui Mudbank (Changjiang Delta) in 1999, through using graduated-stake elevation-monitoring technology (Fan 2001). Sixty-two stakes were fixed on the intertidal ground with a distance of 30–50 m between two neighboring stakes, and they were regularly monitored every single or 2 days. The result shows that net erosion switches on when waves exceed 1.5 m high during non-typhoon conditions (Fig. 9.17). Serious erosion occurs during peak storm periods with a maximum of >15 cm deflations over two to four tidal cycles at some locations (Fan 2001). There are generally existent two erosion zones separated by the accretional zone. It was hypothesized that the erosion and the deposition zones were respectively produced by series of wave breaking and reforming processes over the gentle and broad mudflats (3.4 km wide across entire intertidal zone with a mean tidal range of 2.6 m) before the wave was dying out (Fig. 9.18, Fan et al. 2006). The sites of erosion or deposition change alternatively into deposition or erosion over a next few tidal cycles (Fig. 9.17), denoting the same mechanism that waves tend to break over the previous deposition zones because of shoaling and produce new erosion zones, and vice versa for the previous erosion zones which turn into wave-reforming area to promote deposition.

9.4.1.2 Intermediate Cycles (Neap-Spring Tidal Cycle to Season)

The modulation effect of large-wave processes by tides is significantly different over a single tidal cycle and the neap-spring cycle, exerting great impacts on the tidal-flat development. Tide modulation of storm waves was clearly exhibited by the hydrodynamic data from a field experiment on the Baeksu tidal flats (southwest Korea) in February 1999, where the semidiurnal tidal range varies from 2.3 m at neap to 5.5 m at spring with a mean of ~3.9 m (Kim 2003). The instrumentation system to monitor wave and current was deployed on the lower intertidal flats for 2 weeks, catching two invading winter storms with main wind direction toward the shore. The first storm was stronger than the second in terms of maximum wind speed (~18 m/s vs. ~14 m/s). However, the storm-induced waves were larger for the second (weaker) storm than the first storm in terms of the maximum significant wave height (3 m vs. 2 m). The discrepancy of weaker storm generating larger waves is actually ascribed to the wave-depth relationship, in that the occurrence of weaker storm at spring tide tends to allow larger waves penetrate into the intertidal flats because of higher water depth rising by spring tide, whereas neap tide is potential to damp storm energy more seaward (Kim 2003).

The fact that the intensity of storm-related processes is greatly modulated by the neap-spring cycle was also addressed by Fan et al. (2006) in terms of the erosion magnitude and the distribution of erosion zones across the intertidal flats at the Nanhui Mudbank. They discussed that a weaker storm at spring tides was potential to induce more intense erosion than a stronger storm at neap tides (Fig. 9.18). It is not only due to the higher wave energy and the related mightier vertical scouring capability at spring tides than at neap tides which are determined by water depth as discussed above, but also linked with the higher spring current speed and the related mightier horizontal advection capability than neap tides. Consequently, more sediment is suspended and carried out of the erosion zone by the combined action of storm waves and currents at spring tides than at neap tides, producing higher magnitude of the erosion.

Seasonal alternations of accretion and erosion are the most significant and widely addressed features of the tidal flats (Ren 1985; Shi and Chen 1996; O'Brien et al. 2000; Yang et al. 2005; Fan et al. 2006; Yang et al. 2008b). The processes leading to this periodic development are principally related to seasonal wind climate change, and less to other factors like changes in tidal level, floral and faunal distributions, solar intensity, and estuarine turbidity maximum location. The Baeksu tidal flat in southwest Korea has more

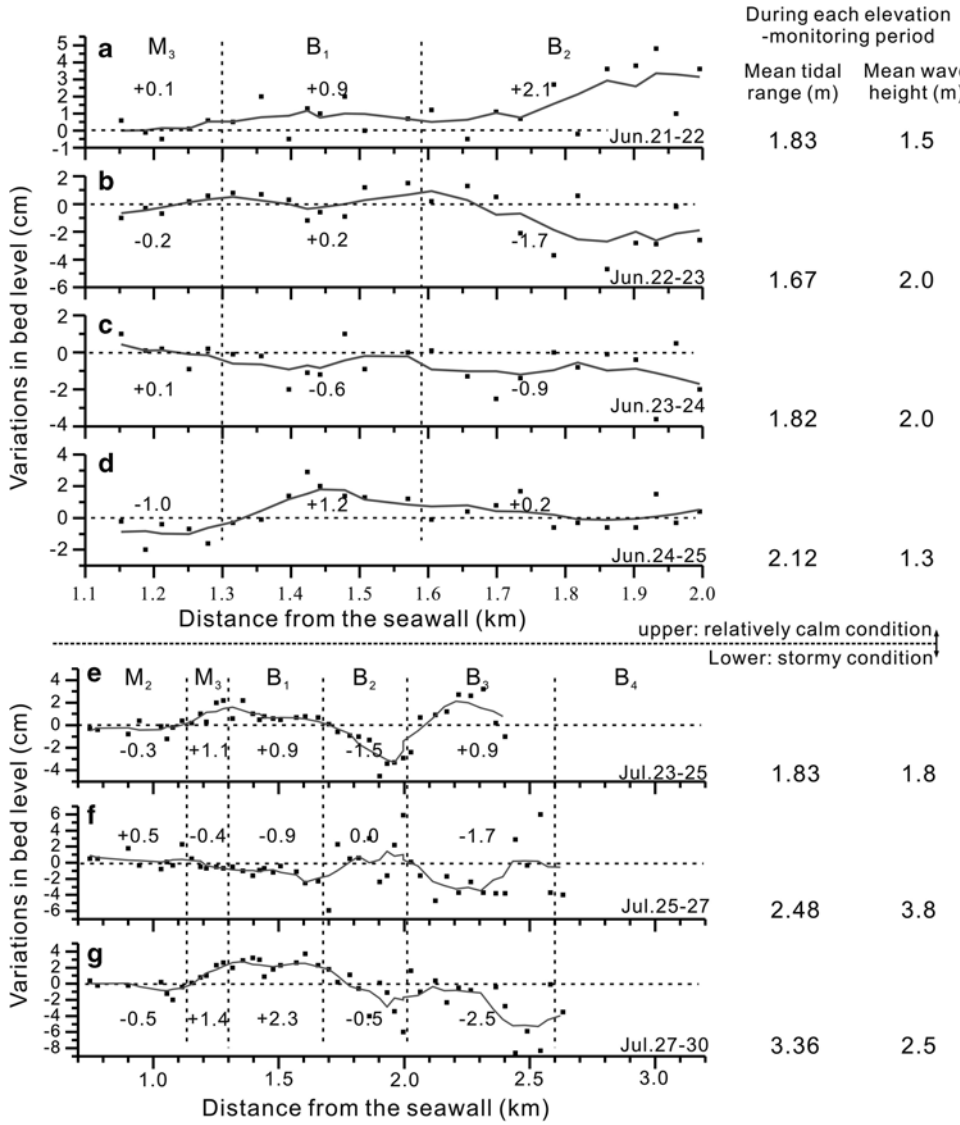

Fig. 9.17 Short-term (1–2 days) variations in bed level of the intertidal flat in the Changjiang Delta (China) over a relatively calm period June 21–25 in 1999 (**a**–**d**) and a stormy period July 23–30 in 1999 (**e**–**g**), respectively. Individual stake measurement data were analyzed by three point adjacent average to generate a smoothed curve, representing a general trend of erosion and deposition across the profile. Different sub-zones of the intertidal flat had different erosion/accretion trends in response to waves. Mean changes in bed level over the different sub-zones were calculated and marked in the figures (After Fan et al. 2006)

frequent and intense storms in winter than in summer, and the resulting seasonal cycles of erosion and deposition are highly contrasting with summer accretional and muddy profile of a normal tidal flat and winter erosional and sandy profile resembling a shoreface (Yang et al. 2005).

Most of the subtropical coast is actually subjected to both summer and winter storms. On the Chongming Eastern Flat (Fig. 9.15), the tidal-flat elevation surveying data showed that the bare flats underwent erosion both in summer and winter (Fig. 9.19). The bare flats were lowered by a few decimeters during sporadic typhoon strikes, and the same magnitude of deposition usually took place soon after the erosion events in summer. By contrast, the winter erosion season began in mid-October with sharp erosion of a few decimeters, and followed with light erosion throughout late March. It lasted for more than 5 months before entering a gradual

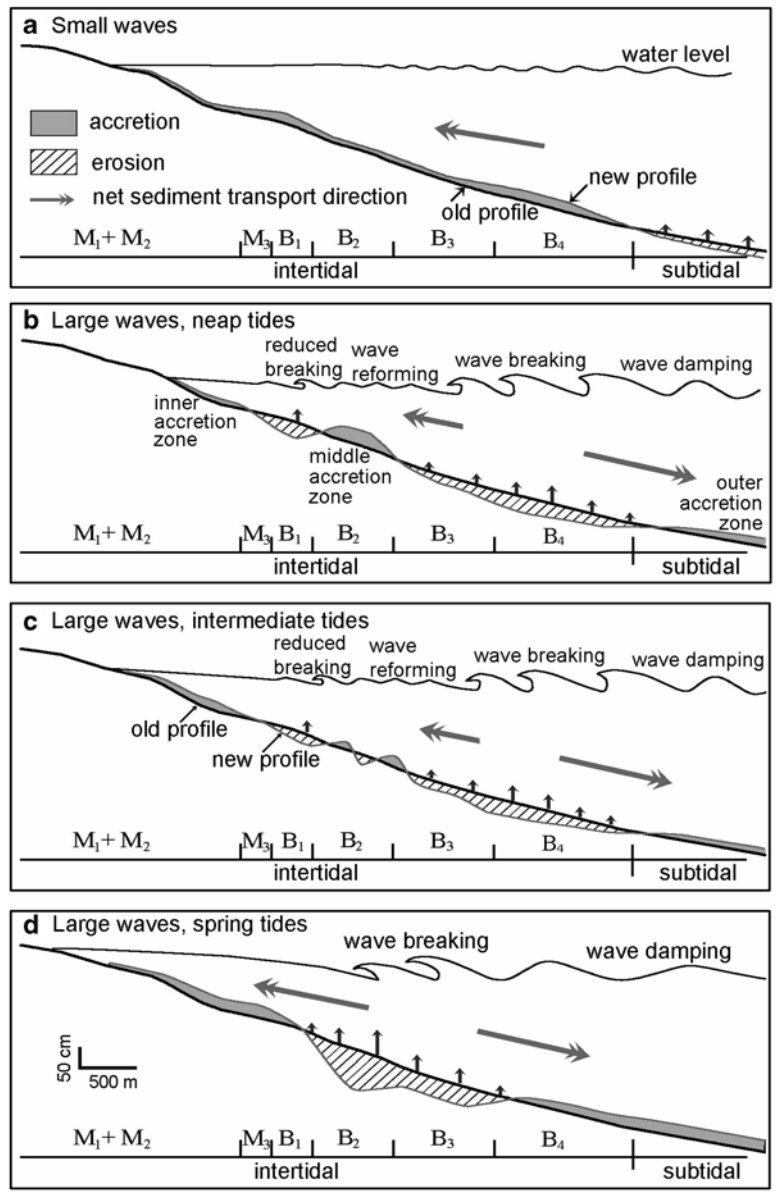

Fig. 9.18 Schematic models showing intertidal morphodynamic processes and sediment transport patterns under different wave and tidal regimes: (**a**) small waves, (**b**) large waves and neap tides, (**c**) large waves and intermediate tides, (**d**) large waves and spring tides (After Fan et al. 2006)

accretion season. It is noteworthy that the salt-marsh land underwent continuous slight accretion throughout the monitoring period, reasonably linked to the protection by the salt-marsh canopy (Fig. 9.19).

The shoreline strike can play important role in the seasonal cycle development owing to the selecting effect of onshore and offshore wind. Along the north bank of the Hangzhou Bay (Fig. 9.7), the east-west orientation shoreline makes the tidal flats sensitive to summer tropical storms with onshore wind domination, whereas sluggish to winter storms with offshore wind domination. This was clearly exhibited by the alternations of the summer sandy erosional flats and the winter muddy accretional flats (Fig. 9.20, Yang et al. 2008c).

Seasonal cycles are also the most outstanding morphodynamic action on the Guiana open-coast tidal flats. The Guiana tidal flats differ from others by their

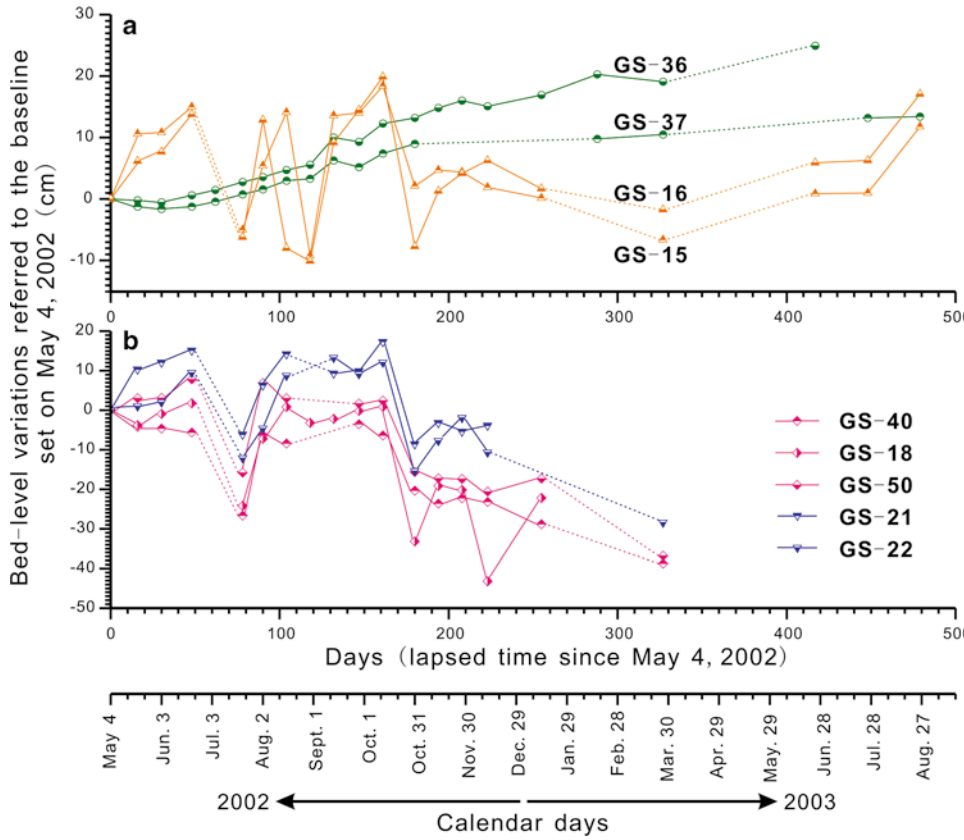

Fig. 9.19 Seasonal variations in bed level of the salt-marsh land and the bare intertidal flats along a northern transect of the Chongming Eastern Flat in the Changjiang Delta. Four groups of elevation-monitoring stakes (GS-36, 37), (GS-15, 16), (GS-18, 40, 50), and (GS-21, 22) are positioned at the lower salt marsh and the upper, middle, and lower bare intertidal flats, respectively. See their detailed locations in Fig. 9.15a

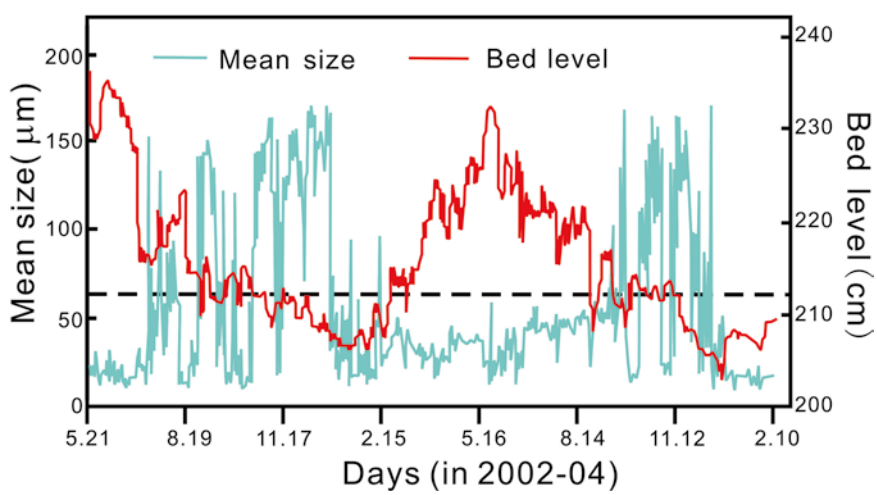

Fig. 9.20 Daily variations in bed level and grain size of surface sediment at a fixed station on the middle intertidal flat along the north bank of Hanzhou Bay. The dash line denotes the division between sand and mud at 63 μm (After Yang et al. 2008c)

typical longshore migration instead of cross-shore evolution (Wells and Coleman 1981; Froidefond et al. 1988; Eisma et al. 1991; Augustinus 2004). There are totally 20–25 mudbanks along the coast of the Guianas (Fig. 9.4), and each is generally 10–40 km in length and several tens of kilometers in width extending gently from the shore to nearly 20-m isobaths (Fig. 9.10). The mudbanks migrate westward, driven by the alongshore current and northwest wind waves generated by trade winds. The mudbank migration is completed by deposition at the leading (western) edge and erosion at the trailing (eastern) edge, which is highly related to the attenuation of the incoming waves significantly by presence of fluid mud at the leading edge or less by presence of the compacted clay deposits at the trailing edge (Fig. 9.10, Wells and Coleman 1981; Allison and Lee 2004). The mudbanks migrate downdrift at mean rates of 0.9–1.5 km year^{-1} (Froidefond et al. 1988; Eisma et al. 1991). Over an annual interval, the windy season from January to April accounts for major sediment exchange between the trailing and the leading edges, producing the most rapid mudbank migration. The annual sediment exchange from the trailing to leading edges along the entire 1,400-km-long Guiana coast adds up to an amazing figure, approximately equal to the average input of new sediment from the Amazon (Allison and Lee 2004).

9.4.1.3 Long-Term Cycles (A Few Years to Decades)

Long-term cycles of tidal-flat developments are commonly envisioned along the deltaic plains/coastal plains, where the shoreline can change rapidly and vastly with a few kilometers or more in a few decades, driven by different mechanisms. Coastal development of the Nanhui Mudbank in the Changjiang Delta was analyzed by using time series of nautical charts from 1842 to 2004 (Fig. 9.21). It was shown that net erosion occurred during the two periods of 1842–1864 and 1911–1958, alternating with two deposition periods of 1864–1911 and 1958–2004. A general erosion/deposition pattern of the mudbank can be summarized as "accretion at the eastern flat with erosion at the southern flat (smaller area)" in the net-deposition periods, and vice versa in the net-erosion periods (Fig. 9.21). It is presumed to mainly result from the coincident shifting of the Changjiang's main channel away (erosion) or toward (deposition) the mudbank. Another pattern was also noted as "accretion at the higher flat (above −2-m) and erosion at the lower flat (below −2-m)" in the net-deposition periods, especially during 1864–1911, whereas a reversed pattern of "erosion at the higher flat and accretion at the lower flat" occurred in the net-erosion periods, especially during 1842–1864 (Fig. 9.21). The alternations of erosion and deposition phases between the higher and lower flats were presumably linked to multi-decadal alternations of the frequency of intense tropical storms. In other words, the coastal morphology tends to preserve the storm-induced profile in terms of "erosion at the higher flat and accretion at the lower flat" in the stormy decades, whereas the normal-wave morphology with "the higher flat accretion vs. the lower flat erosion" is cumulatively present in the relative calm decades (Huo et al. 2010).

The multi-decadal variations in the Guiana coastline are produced by its typical alongshore migration of series of the mudbank and the interbank units, which continuously pass through a given location (Fig. 9.22). The mudbanks migrate with an average rate of 1.5 km year^{-1} along the Surinam coast, and the average alongshore width is 45 km for each geomorphologic unit including a mudbank and the neighboring interbank area (Fig. 9.10). It is therefore estimated a roughly 30-year cycle of erosion and deposition along the Surinam coast (Augustinus 2004). Due to huge sediment input from the Amazon, a net coastal-plain growth is generally produced after each mudbank-interbank cycle (Fig. 9.22, Allison and Lee 2004). It was noteworthy that the comparison studies using historical maps and Holocene core data demonstrated the difference between the present and Holocene sedimentary processes of the mudbanks. The present, roughly 30-year cycle of high rates of accretion and erosion associated with the mudbank migration extended at least as far back as the last two and a half centuries, but the beginning of this cycle is still uncertain (Plaziat and Augustinus 2004).

There was reported to exist another multi-decadal cycle of erosion and deposition along the Guiana coast, driven by secular change of ocean wind and wave climate (Eisma et al. 1991; Allison et al. 2000; Augustinus 2004). A comparison study of different ages of air photographs showed that the Surinam coast changed as a whole from net erosion during the period 1947–1966 to net deposition in the period 1966–1981 (Fig. 9.23, Table 9.2). The change was found coincidently with an increase in mean wind velocity and a general shift of wind direction from

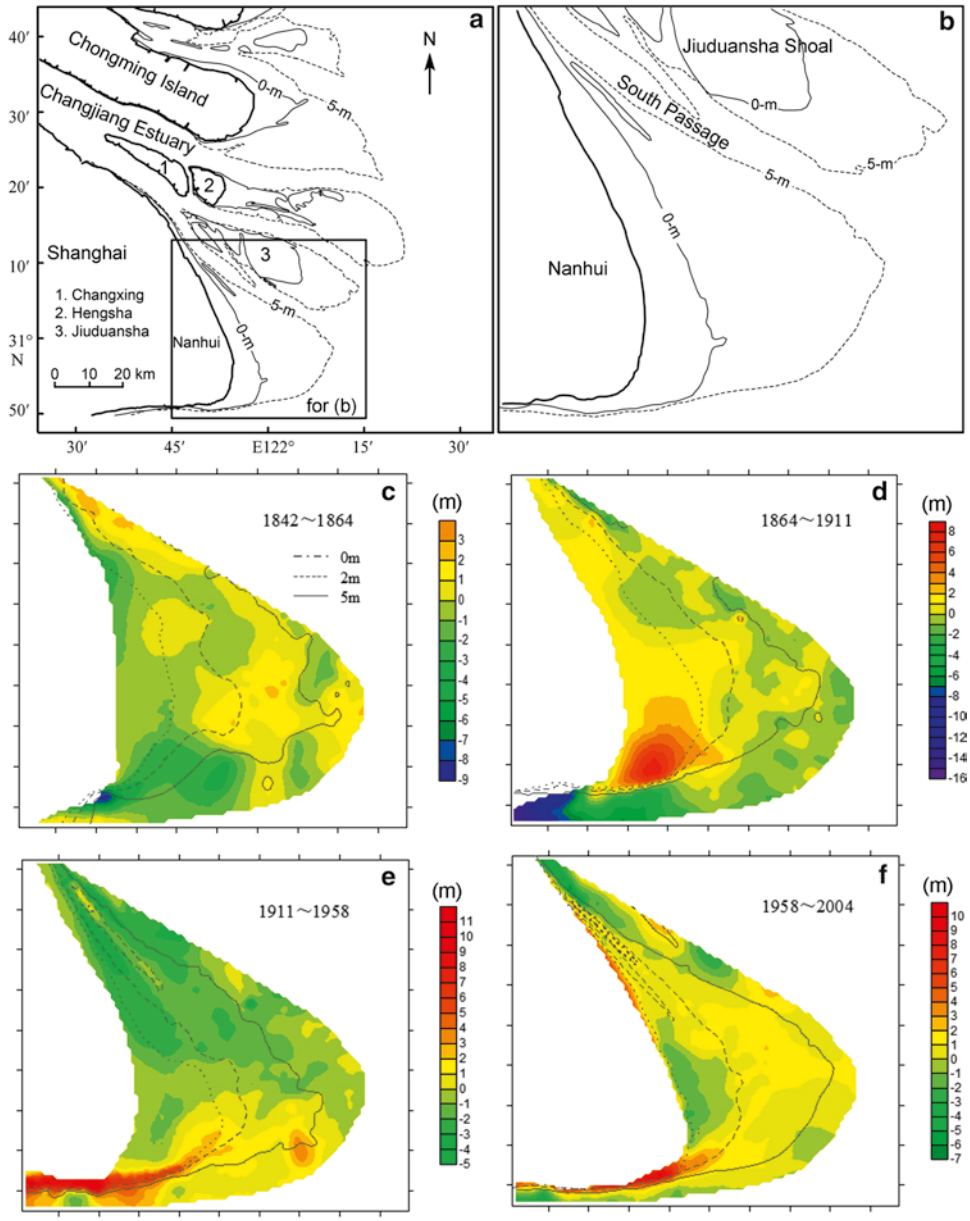

Fig. 9.21 Multi-decadal coastal development of the Nanhui Mudbank in the Changjiang Delta (After Huo et al. 2010). Color bars denoting the magnitude of accretion (positive) and erosion (negative)

more NE to more ENE from 1959 onward. The stronger winds and the change in direction toward a smaller angle with the coastline resulted in an enhanced alongshore transport and a reduction of the onshore wave energy component. This led to net deposition in the Surinam coast (Eisma et al. 1991). Enhanced alongshore transport also favored development of longer mudbanks (Fig. 9.23, Augustinus 2004). Multi-decadal changes in the Guiana coastal development were therefore presumed to be determined by the variations in the strength and the direction of the trade winds instead of the flux of sediment supply from the Amazon (Eisma et al. 1991). Note that the coast of Guiana and French Guiana has an SE-NW orientation, different from the nearly east-west orientation of the Surinam coast. The difference in angle

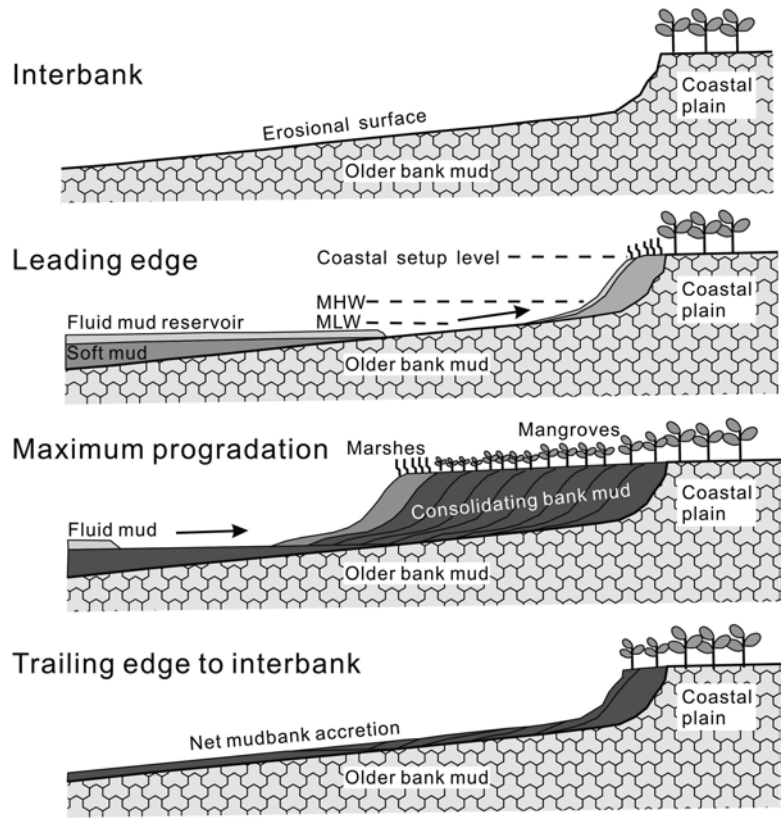

Fig. 9.22 Schematic model for shoreline evolution cycles in the Guiana coast. Serious erosion takes place at the interbank phase (*top panel*). It is succeeded by leading edge mudbank deposition (*second panel*). The accretion continues till the passage of the leading edge to reach the maximum progradation (*third panel*). And erosion takes place again by the swing of the trailing edge (*bottom panel*). Note that there is a net coastal plain growth with each mudbank-interbank cycle (After Allison and Lee 2004)

between the coastline and the direction of wave propagation accounts for the different behaviors of the respective mudbanks. Consequently, the mudbanks in Guiana are shorter than those in Surinam, and their behaviors are more erratic than the latter (Eisma et al. 1991; Augustinus 2004).

9.4.1.4 Megacycles (Hundreds to Thousands of Years)

Mega-scale coastal development is referred to the geological evolution of the Holocene coastal plains over a time scale of centuries to millennia. It is generally addressed through using cores or large-scale coastal morphological features. Chenier ridges are typical and extensive features on coastal plains near the mouths of rivers (typically large rivers), excellent indicator for the ancient coastline location and evolution (Meckel 1975; Liu and Walker 1989; Wang and Ke 1989; Lees 1992). They demarcate the flat coastal plains with coastline-parallel ridge series, mainly composed of sand and shell debris, a few decimeters to meters higher than the surround mudflat/marsh deposits. There are generally four chenier ridges along the western coastal plain of the Bohai Bay, five in the North Jiangsu coastal plain, and eight in the Changjiang Delta (Fig. 9.13). The oldest chenier in the Changjiang Delta and the North Jiangsu coastal plain was dated 6,460 year BP and 6,160 year BP, respectively. The two chenier plains were therefore assumed to begin to develop since the mid-Holocene maximum flooding period, but have afterward been interrupted several times to produce other cheniers.

The chenier formation represents an episode of erosion, whereas the intervening mud deposition represents a period of coastal progradation. The development of chenier plains is generally presumed to mainly result from sediment starvation by the distributary channel switching (Lees 1992). The lower reach of the Huanghe switched several times between debouching into the Bohai Bay and the Yellow Sea, accounting for the formation of the cheniers on the western coastal plain of the Bohai Bay and the North Jiangsu coastal plain (Liu and Walker 1989; Wang and Ke 1989). Each chenier on the southern coast of the Changjiang Delta was formed when the Changjiang main channel switched north and away from the south bank. The same mechanism was also

employed to interpret the chenier development in the Mississippi Delta (Byrne et al. 1959) and the Colorado Delta in the Northern Gulf of California (Meckel 1975).

Sediment starvation for a coast can also result from a reduction in fluvial input from the drainage basin instead of the delta channel switching. The chenier ridges on the coastal plains of North Australia were presumably formed during low mud influx accompanying the long-term dry periods in the drainage basins, while mudflat deposition occurred during the wetter periods (Rhodes 1982; Lees 1992).

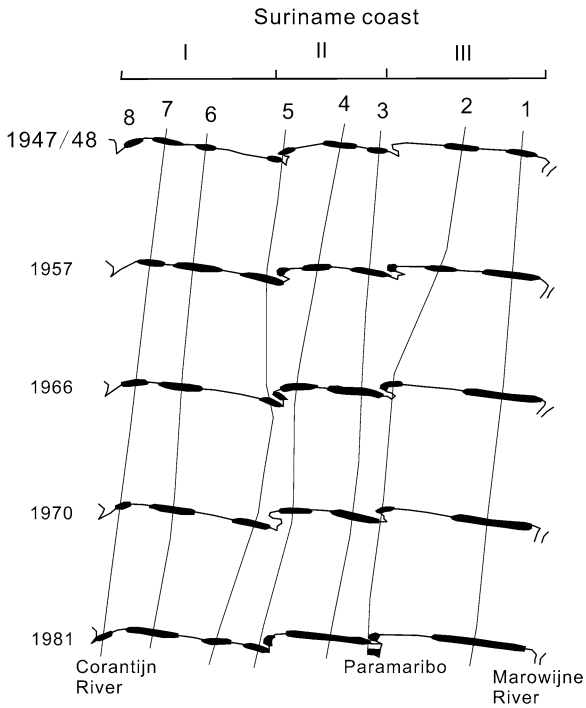

Fig. 9.23 Changes in position and length of the mudbanks (*heavy lines*) along the Surinam coast between 1947 and 1981 (After Eisma et al. 1991)

The formation of cheniers could have resulted from not only the reduced sediment availability but also the increased energy of marine processes. There are two series of well-developed chenier bundles on the Surinam coastal plain, denoting that the coastal development was interrupted at least twice by longer intervals of erosion during the Coronie Formation (<6,000 year BP). These two hiatuses among the three sedimentation phases of Wanica, Moleson, and Comowine coincided with a slight drop in sea level (Fig. 9.14) and a systematic increase of more northerly wind frequencies. The chenier formation is therefore simply considered to link with the more northerly wind frequencies and a fall in sea level (Eisma et al. 1991; Augustinus 2004).

9.5 Sedimentary Structures and Bedding

Bedforms and sedimentary structures are highly related to sediment size and hydrodynamics (Boguchwal and Southard 1990). Open-coast tidal flats vary greatly in major grain-size composition from fine silt to sand (Table 9.3). Wave energy can be dissipated higher or less when propagating over the muddy or sandy flats due to presence of fluid mud or not, and the wave is also greatly modulated by tidal fluctuations. The difference

Table 9.2 Total amounts of mud yearly eroded (−) or deposited (+) along the Surinam coast over different periods (After Eisma et al. 1991)

Period	Section	Total amount ($\times 10^8$ tons)	Amount per year ($\times 10^6$ tons year^{-1})	Net amount over the entire coast ($\times 10^6$ tons year^{-1})
1947–1957	I	−15.90	−1.59	
	II	+9.85	+0.99	−0.82
	III	−2.09	−0.21	
1957–1966	I	−14.19	−1.58	
	II	+0.45	+0.05	−1.00
	III	+4.71	+0.52	
1966–1970	I	+6.55	+1.64	
	II	+1.28	+0.32	+2.18
	III	+0.89	+0.22	
1970–1981	I	+30.85	+2.81	
	II	+44.57	+4.05	+7.61
	III	+8.29	+0.75	

Table 9.3 Typical sedimentary structures on the open-coast flats

Types of tidal flats			Muddy flats					Sandy flats
Examples			The coast of the Guianas	Northwestern Gulf of California	The Fly Delta, Papua New Guinea	Kyonggi Bay and Namyang Bay	Wanggang tidal flats, Jaingsu Province, China	Baeksu, Doowoori, and Dongho tidal flats, Korea
Grain size			Silty clay	Clayey silt to silty clay	Mean percentiles of sand, silt, and clay are 29.4%, 53.2%, and 17.4%	4.3–5.8 ϕ in Kyonggi Bay; 4.6–8.8 ϕ in Namyang Bay	4.38–6.25 ϕ	Seasonally changing from 4–5.5 ϕ in summer to <3–4 ϕ in winter
Zonations	Supratidal flat		Mangrove occupied; massive beds with abundant roots and benthic traces	Not distinct laminations or beddings; prevalent mud desiccation and salt crystallization; rare shell fragments	Mangrove and salt marsh occupied; prevalent homogenous mud; infrequent thin interlayered laminations	Absent	Salt marsh occupied; intense bioturbation of original parallel to slight-wavy laminations	Absent
	Intertidal flats	Upper		Common laminae; some small-scale cross-beddings in sand; common burrows; fine shell hash in sandy laminae and complete mollusk shells in mud		Intense bioturbation of original wavy beds; infrequent flaser beds, clasts, and convolutions	Interlayered beddings of thick mud layers and thin sand layers; common parallel laminations in the mud beds and small ripple laminations in the thick sand beds; intense bioturbation	Interlayered bedding of winter sand deposits and summer mud deposits and the features preserved in the strata
		Middle	Common massive beds and parallel to subparallel laminations; some wavy laminations; rare lenticular laminations, micro-cross-laminations, scour and fill structures, and biogenetic traces		Prevalent planar to wavy laminations; common soft sediment deformation; sand layer thickening and coarsening as decreasing elevation; limited bioturbation	Common parallel to wavy beddings; infrequent ripple and parallel laminations; slight bioturbation	Interlayered beddings of thick sand layers and thin mud layers; common wave beddings in the thick sand layers; coarser sediment in the tidal creeks containing bipolar cross-beddings	The summer muddy flat with interbedded sand and mud, changing into the winter sandy flat prevalent sandy parallel laminations and hummocky cross-stratification; the strata preserved majorly the winter storm coarse deposits with little bioturbation
		Lower				Prevalent small ripple laminations, intense bioturbation		
	Subtidal flat/ channel			Thin laminae, typically lenticular and irregular	Prevalent interbedded sand and mud; present ripple cross-laminations and slump features	Common thick cross-stratification, slightly mottled to better stratified	Thin parallel to wavy beddings; presence of small cross-beddings and herringbone cross-beddings	Sediment finer than the lower intertidal flat
Sedimentation rates over a 100-year scale			Several millimeters to centimeters	A few centimeters	A few centimeters to decimeters	A few millimeters	A few centimeters	≤1 mm
Major references			Rine and Ginsburg, (1985); Allison et al. (1995a, b)	Meckle (1975); Thompson (1975)	Baker et al. (1995), Walsh and Nittrouer (2004)	Frey et al. (1989); Alexander et al. (1991), Park et al. (1995)	Ren (1985)	Yang et al. (2005, 2008b)

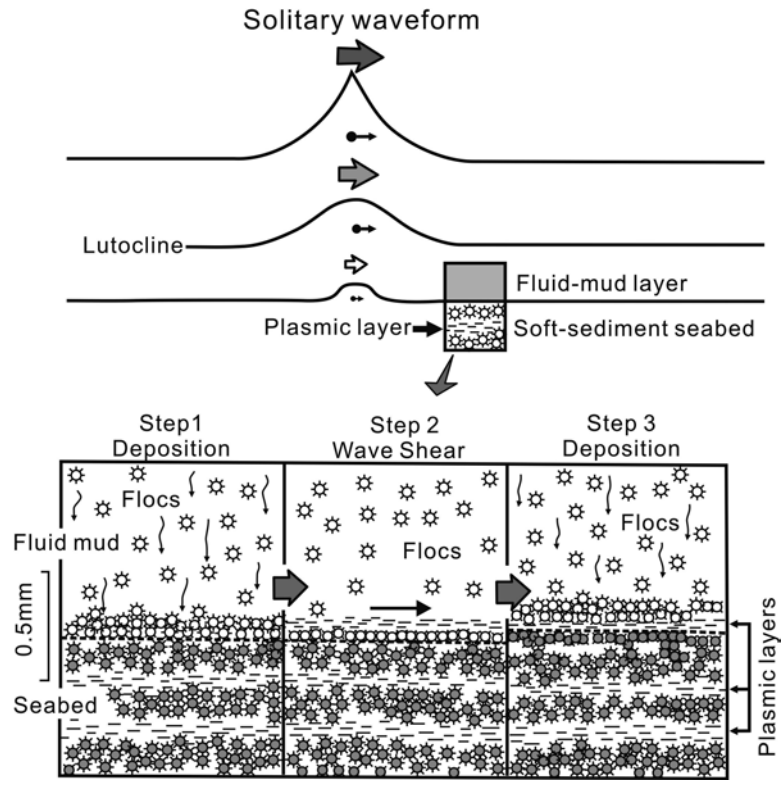

Fig. 9.24 Schematic model for the genesis of plasmic fabric layers (~0.01–0.1 mm thick) on the muddy banks along the coast of Guianas. Because of the viscosity difference, shear is produced at the boundary of fluid mud and sediment with passage of solitary wave crests (*upper panel*). The shear is considered to break the surface flocs and orient platy mineral grains, creating a plasmic layer. Between weaves, floc deposition is possible, producing unoriented interlaminations (After Allison et al. 1995a)

in grain size and combined wave-current energy consequently determine the sedimentary character changing in a spectrum from the wave-influenced, tide-dominated on the muddy (fine silt domination) open-coast tidal flats, through the wave- and tide-dominated on the muddy (coarse silt domination) open-coast tidal flats, to wave-dominated on the sandy open-coast tidal flats. The spectrum change is also evident in the strata with increasing volume of storm deposits from the muddy to sandy open-coast tidal flats.

The mudbanks along the Guiana coast are muddy open-coast tidal flats, predominantly consisting of fine silt and clay. The prevalent bedding is massive beds, or parallel to subparallel laminations of a few micrometers to millimeters thick (Table 9.3; Rine and Ginsburg 1985; Allison et al. 1995b; Allison and Lee 2004). The millimeter-scale laminations of silt enrichment are commonly layered structures in X-radiographs. The micrometer scale of the structures should be examined in thin sections under microscopes, named plasmic or unistrial fabric (Kuehl et al. 1988; Allison et al. 1995a, b). The plasmic fabric is composed of alternating layers (about 0.01 mm thick) of oriented and unoriented clay and mica with the oriented layers showing uniform extinction under polarized light. The formation of plasmic fabric was presumed to result from in situ shearing by surface gravity waves in sediments being rapidly deposited from a fluid-mud suspension (Fig. 9.24, Rine and Ginsburg 1985; Allison et al. 1995b). Solitary waves have almost unidirectional flow approaching the shore (Wells and Coleman 1978). Because of the viscosity difference, passage of solitary waves induces shear along the fluid mud/sediment boundary. This shear is postulated to break flocs and orient platy particles (micas and clays) in the direction of shear. Floc deposition takes place between waves, producing unoriented interlaminations (Allison et al. 1995a). The plasmic fabric is the finest scale of sedimentary structures having wave imprints as known so far, but it is difficult to be distinguished in fossil rocks and linked to wave generation.

Most of the muddy open-coast tidal flats are predominantly composed of silt, with small fractions of clay and fine sand (Table 9.3). The preferred surface structures are small ripples on the muddy flats if no presence of storm waves. On the Chongming Eastern Flat in the Changjiang Delta, small symmetrical wave ripples and combined flow ripples are the commonest

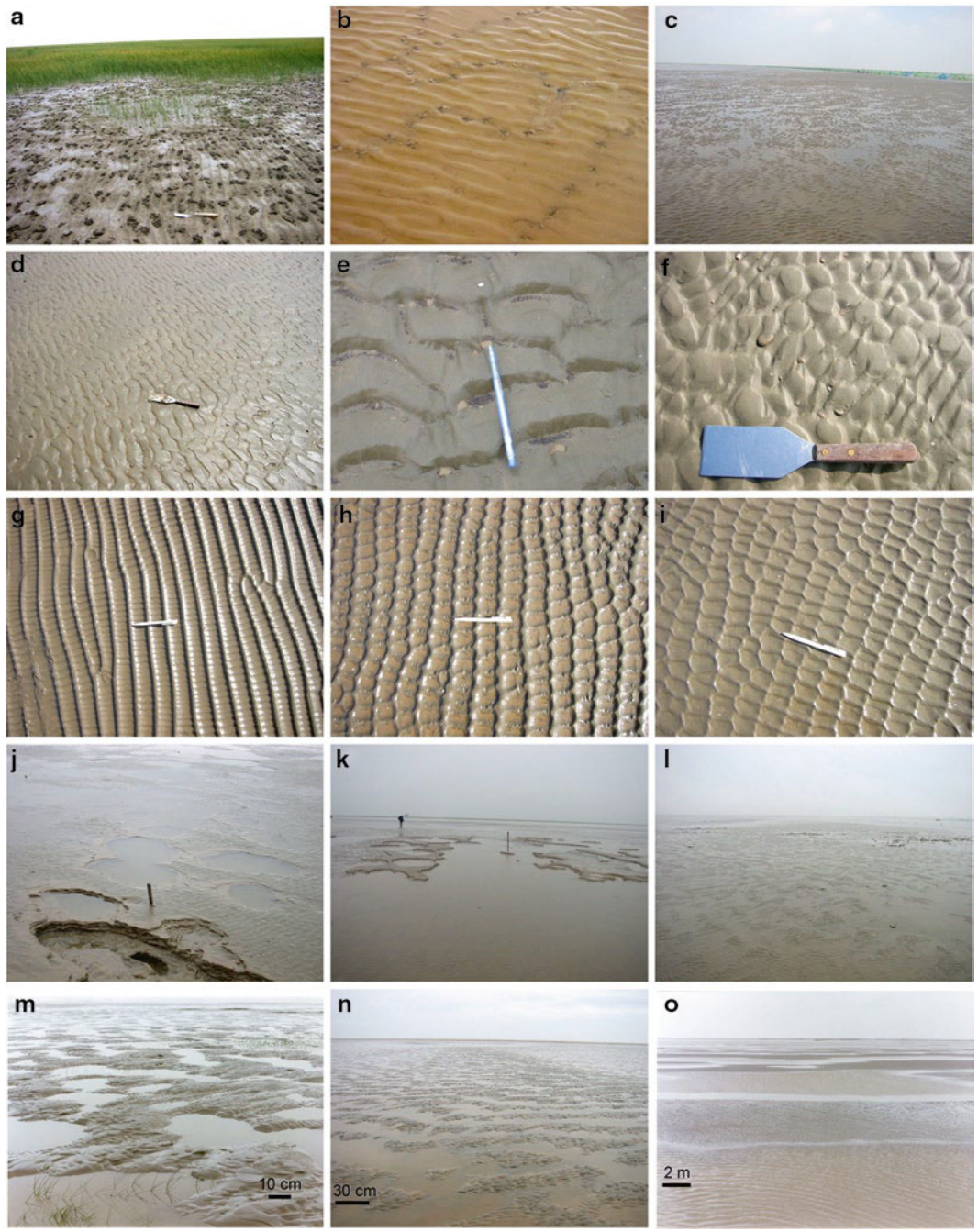

Fig. 9.25 Surface structures on the Chongming Eastern Flat of the Changjiang Delta. Small symmetrical wave ripples on the marshland (**a**) and on the upper bare flat (**b**). Small combined-flow ripples on the bare flat (**c**–**f**) including the flatten-crested ripples (**d**) and undulatory to lingoid current ripples (**e**, **f**). Interfering ripples with the coast-parallel straight-crested ripples increasingly modified by orthogonal waves seaward from (**g**) to (**i**); ballpoint pen is 14 cm long and pointing toward the sea. Increasing wave reworking on the muddy flat to produce small separate erosion holes (**j**), broaden and connect the holes, turn muddy deposited layer into patches (**k**), and develop the embryonic dunes (**i**) and well-developed dunes topped by small ripples on the marsh-frontal zone (**m**) and the middle and lower intertidal flats (**n**, **o**)

bedforms (Fig. 9.25a–f). Interfering ripples are also frequently present, with the modification magnitude of one group of wave ripples by another increasing seaward from the upper to the lower bare flats (Fig. 9.25g–i). Accumulation of these small rippled beds tends to produce lenticular and wavy bedding, which is commonly seen on the tile sedimentation and along the erosion cliff of remnant muddy patches (Fig. 9.26). On the fortnightly (one neap-spring-neap cycle) tiles, 3–6-cm-thick deposits were not found to have direct link with neap-spring cycles in terms of lamina number and thickness variation (Fig. 9.26e–h), even the extrapolated sediment rate reaching up to 72–144 cm $year^{-1}$. It is reasonably linked with the formation of rippled laminae, lenticular and wavy bedding by waves or combined wave and tide flows instead of purely tides (usually known as tidal bedding, Reineck and Singh 1980), and thicker and sandier laminae represent higher energy events of larger waves or the combined flows of larger waves and higher tides instead of purely higher tides.

The muddy open-coast tidal flats can temporarily shift into sandy flats during the storm conditions, developing erosion features, dunes, and storm-generated bedding. On the Chongming Eastern Flat, erosion by rising storm waves starts at discrete points, and the erosion holes gradually expand to unite each other until there are only a few isolated muddy patches on the sandier deflated flats, following with the bedforms growing from small ripples into large dunes (Fig. 9.25j–o). Storm decaying initiates to deposit first a sandy lag layer with abundant shell debris and mud pebbles over the erosion surfaces, and follows with a thinning- and fining-upward succession, that both grain size and thickness of sandy laminae decrease upward, gradually returning the normal tidal-flat thinly interlayered deposition (Fig. 9.27). During a storm season, previous storm deposits tend to be reformed by the following storms, producing a single amalgamated storm-deposited succession. For example, units b, c, and d were deposited by typhoons Neil, Olga, and Paul, respectively, over the typhoon season in 1999; the former two units were the remnants by subsequent storm reworking (Fig. 9.27; Fan et al. 2004a). A thinning- and fining-upward succession is therefore a storm-related small succession consisting of a lower half of sand-dominated layers (SDLs, storm deposition) and an upper half of mud-dominated layers (MDLs, after storm, normal tidal-flat deposition). The small storm-related succession usually has approximately half-and-half ratios of SDLs and MDLs, commonly seen in the Changjiang Delta where a high sedimentation rate is generally achievable with several centimeters per year (Li et al. 2000; Fan and Li 2002).

The deposits of sandy open-coast tidal flats may consist predominantly of high-energy storm deposits with volumetrically minor amounts of tidally induced lamination (Yang et al. 2005, 2008a). The Baeksu sandy flats in southwest Korea were finely explored by Yang et al. (2005, 2006, 2008a, b). In summer lower energy season, the flats are commonly veneered by mud layer of several centimeters thick, consisting of thinly interbedded to interlaminated sand and mud. The mud layer can be partitioned into two to three smaller-scale upward-fining successions, interpreted as weak summer storm deposits (Fig. 9.28). In winter higher energy season, the flats turn into sandy substrate topped by dune field. The deposits contain extensive wave-generated parallel lamination and short-wavelength (0.3–2 m) hummocky cross-stratification (HCS, Table 9.3, Fig. 9.28), highly similar with those of shoreface facies. Yang et al. (2008a) suggested that the storm deposits on the sandy open-coast tidal flats contained evidence of tidal modulation of storm processes, in which single storm layer is composed of three distinctive rippled intervals: (1) landward-dipping, ripple cross-lamination at the base, produced by combined flows during rising tide; (2) symmetrical buildup of wave-ripple cross-lamination in the middle, formed by oscillatory wave motion at high tide when currents are weak; and (3) seaward-dipping, ripple cross-lamination at the top, deposited by combined flows again during falling tide. Because of limited input of fine sediments and lower sedimentation rate, the summer muddy laminated successions were less preserved, leading to the strata mainly composed of winter sandy deposits with typical HCS (Yang et al. 2005).

It is generally concluded that deposits of open-coast tidal flats are characterized by abundant sedimentary features generated by waves or combined flows, making them distinctly different from the sheltered tidal flats. The features of tidal modulation of wave action distinguish them from the shoreface facies. The most extensive cyclic successions are strongly asymmetric with only the upper half of a fining-upward cycle (Figs. 9.27 and 9.28), denoting the annual depositions of seasonal prevalent large waves alternating with small waves (Baker et al. 1995; Li et al. 2000; Dalrymple et al. 2003; Fan et al. 2004a; Yang et al. 2005).

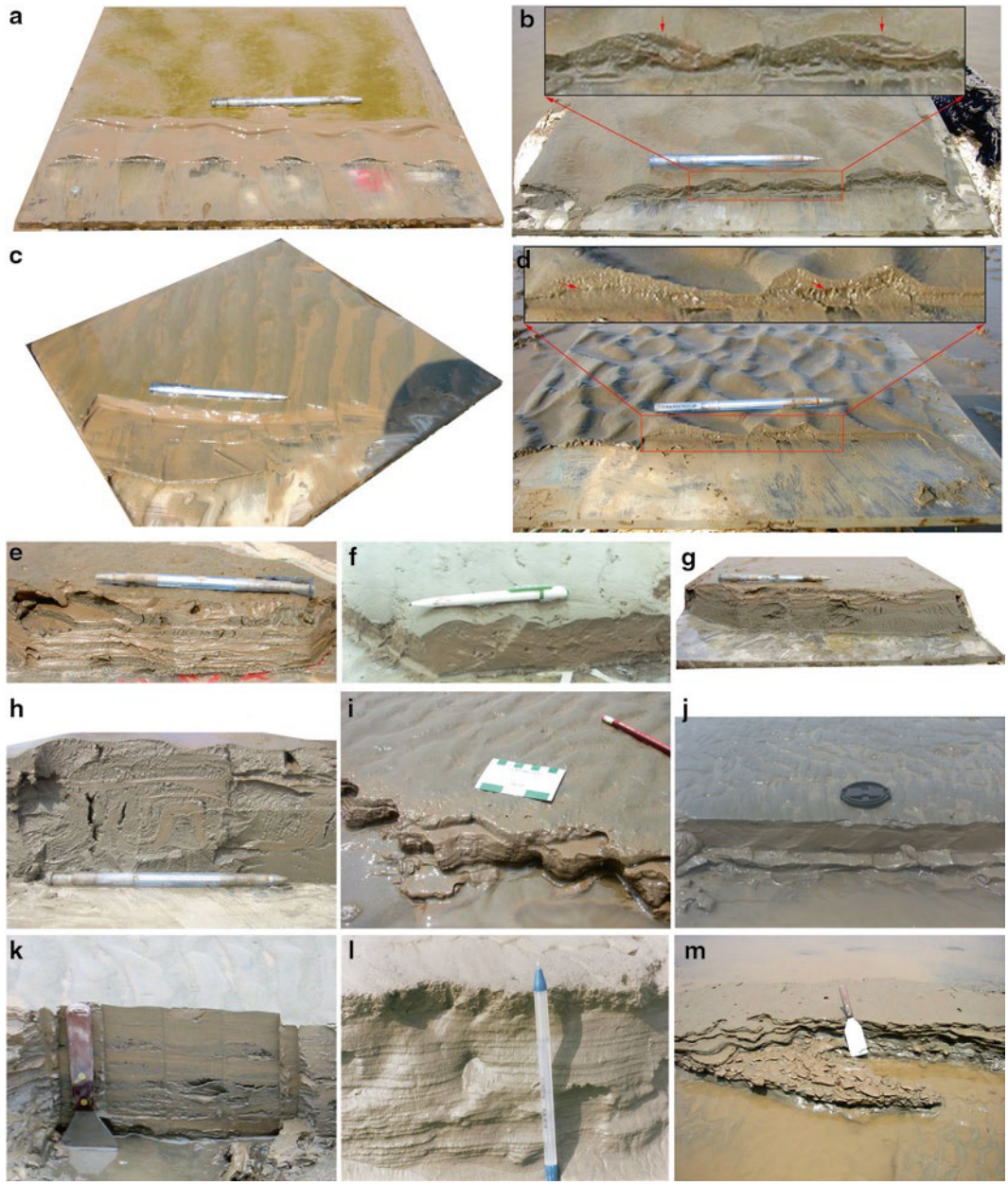

Fig. 9.26 Sedimentary beddings and internal structures of the tidal-flat deposits in the Changjiang Delta. Semidiurnal tile observations showing (**a**) one sand-mud couplets pair with small symmetrical wave ripples capped by a thick frozen fluid-mud layer and a thin algal mat on the surface, and (**b**) two sand-mud couplets with the ebb-current ripples laid on the stoss-side of the underlying flood-current ripples. Diurnal tile observations exhibiting two thin sand laminae separated by a thick mud layer (**c**), or by a hiatus surface with different color and composition (**d**). On the fortnightly observation tiles, 3–6-cm-thick deposits consisting of ≤7 sand-mud couplets, exhibiting thinly interlayered bedding (**e**); two thin sand layers sandwiched by a thick mud layer with a few thin sand lenses (**f**); fining-upward successions with massive sand layer at the bottom and parallel to wavy beddings on the *top* (**g**), or developing load structures with the lower heterolithic bedding (**h**). The erosion cliff of the mud patches showing finely laminated bedding (**i**), fining-upward succession with parallel to wavy bedding (**k**, similar with (**g**) and (**h**) on the fortnightly ties), and thick massive mud layer capped by thin sand layer (**j**, like those of (**f**)). The underlying sandy deposits exposed by deep erosion containing parallel bedding (**l**) and mud-pebble concentration layer (**m**). Ballpoint pen always pointed to the sea

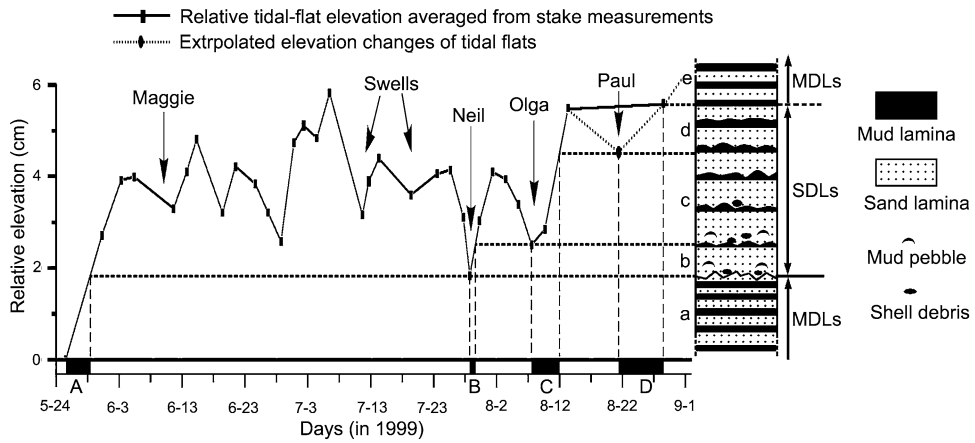

Fig. 9.27 Genesis interpretation of a small succession consisting of sand-dominated layers (*SDLs*) and mud-dominated layers (*MDLs*) using elevation-monitoring data at the Nanhui Mudbank, the Changjiang Delta. The net sediment increments (*a–d*) in the right column were deposited at the time intervals (*A–D*) in the bottom column. Maggie, Neil, Olga, and Paul are names for four typhoons having exerted great impact on the study area in 1999 (After Fan et al. 2002, 2004b)

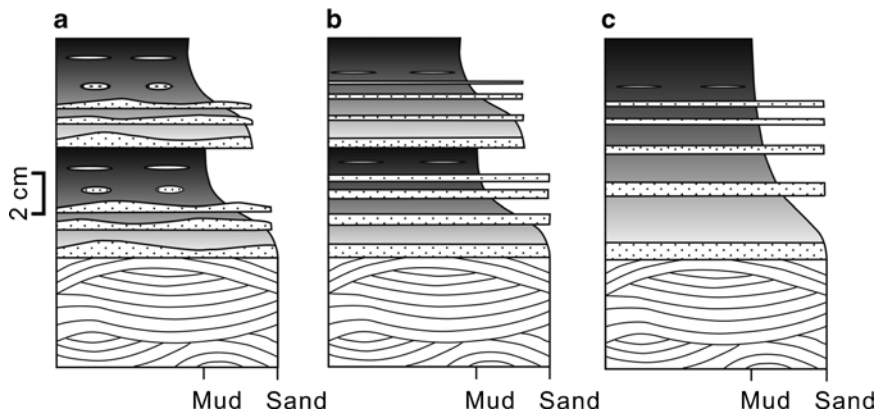

Fig. 9.28 Sketch drawing of the superposition of the winter large-wave coarse deposits and the summer weak-wave fine deposits. The coarse-bedding package characteristic of hummocky cross-stratification (*HCS*) was formed during the waning stage of bigger storm. The fine-bedding package was composed of one or two smaller upward-fining successions, each succession presumably being formed during the waning stage of smaller storm and during the immediate post-storm period in summer (After Yang et al. 2005)

9.6 Preservation Potential

Preservation potential of the deposits is general very low on the open-coast tidal flats due to frequent reformation by waves, especially storms. It has be recently studied by the preservation potential of individual couplets, ratios of gross and net sedimentation rates, and numerical modeling (Li et al. 2000; Fan 2001; Fan and Li 2002; Gao 2009).

Sand-mud couplets are basic sedimentary units of tidal-flat deposits, and their formation and preservation potential have been extensively discussed by a series of field observations in the Changjiang Delta (Li et al. 2000; Fan 2001; Fan et al. 2001, 2002, 2004b; Fan and Li 2002). The method is simply based on the comparison study of number and thickness of couplets using the tile observation. A group of tiles were fixed closely on the tidal-flat surface and regularly visited by different time intervals spanning from a semidiurnal tide to a month or longer (Fig. 9.29). Two couplets were sometimes observed to accumulate on the semidiurnal tile, denoting both flooding and ebbing flows potential

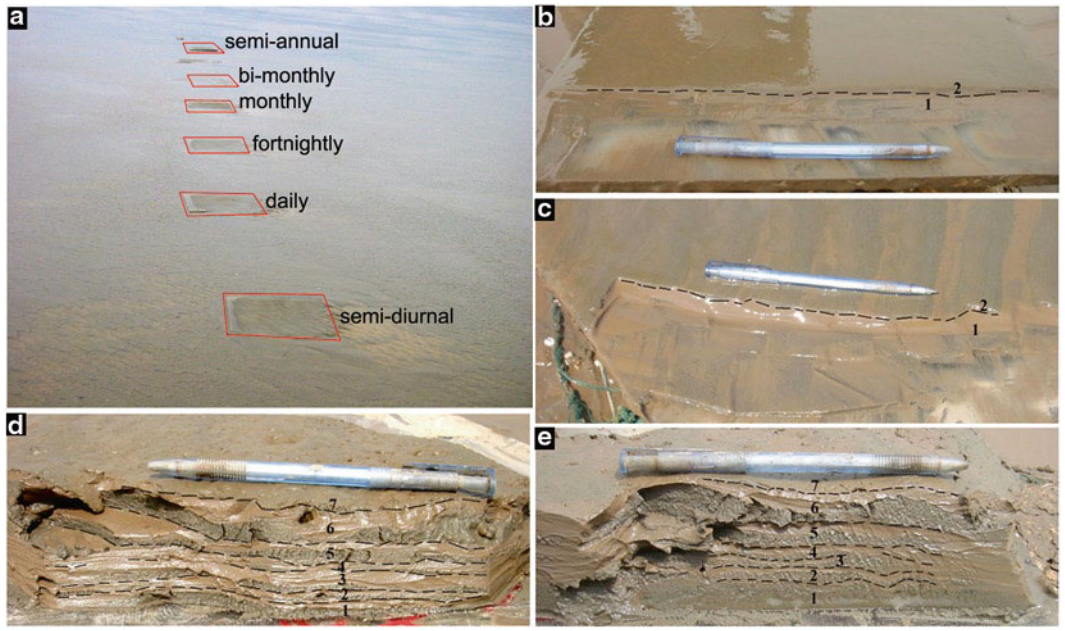

Fig. 9.29 Sedimentation on the observation tiles (40-cm wide and 40-cm long) visited by regular intervals spanning from a half day to a month or longer. The field monitoring experiment was carried in 2002 with six tiles fixed on the middle intertidal-flat surface at the same time, and each tile was scheduled to visit and redeploy at different time intervals spanning from a half day to six months (**a**). However, the bi-monthly and semiannual tiles were taken away by waves after 6–7-week deployment, so no record was available from these two tiles. Photos (**b**–**e**) showed examples of sedimentation on the tiles. There are two sand-mud couplets on the semidiurnal and daily tiles (**b** and **c**) and seven couplets on the fortnightly and monthly tiles (**d** and **e**). The dashed line marks the couplet boundaries. The ballpoint pen is 14 cm long, and pointing toward the sea (After Fan et al. 2004a)

to form their own couplets. In the period from May 4 to June 4 in 2002, there were cumulatively 55, 13, and 7 couplets observed on the daily, fortnightly, and monthly tiles, respectively (Fan et al. 2004a). Compared to the maximum of 120 couplets potentially deposited by 60 semidiurnal tides in the period, the preservation rates of couplets were 45.8%, 10.8%, and 5.8%, respectively, for the daily, fortnightly, and monthly intervals. It is indicated that the preservation rate of couplets decreases rapidly as time intervals increase (Fan et al. 2004a). The same conclusion has been achieved from the tile observation experiment in 1999 at the Nanhui Mudbank (Table 9.4, Fan and Li 2002). Based on the core study, Li et al. (2000) further extrapolated that the preservation rate of couplets could be lowered to 0.2% over a 100-year scale. Also, the sedimentation rates calculated over different time intervals decrease exponentially as the time intervals increase (Table 9.4, Fan et al. 2001).

The problem of the low spatial resolution of the preservation potential studies by in situ measurements can be effectively solved by numeric modeling. A forward modeling approach has been employed to simulate the preservation potential of tidal-flat deposits on the North Jiangsu coast (Fig. 9.11, Gao 2009). The results showed that the preservation potential was the highest over the upper part of the intertidal flat and the lower part of the subtidal flat, and the lowest near the mean sea level and the mean low water springs (Fig. 9.30). Also, the preservation potential decreased as the tidal flats prograded seaward. The slope of tidal flats has significant influence on the preservation potential, in that the minimum value is approximately four times greater for the slope scenario of tan $\beta = 0.5 \times 10^{-3}$ than that of tan $\beta = 1.0 \times 10^{-3}$ (Gao 2009). The simulation result of the preservation potential is comparable with those from field experiments in the Changjiang Delta (Li et al. 2000; Fan 2001; Fan and Li 2002).

The lower preservation rates indicate that the intertidal-flat deposition is riddled with various diastems. The incompleteness of tidal-flat deposition has been explored in detail along the 4-m-thick intertidal-flat deposition in the Changjiang Delta (Fan et al. 2002). The 4-m-thick strata were extrapolated to deposit in

Table 9.4 Comparison of couplet number and thickness on the daily and fortnightly tiles for the field observation on the Nanhui Mudbank in the Changjiang Delta during the period May 24 to July 8 in 1999 (After Fan and Li 2002)

	Daily tiles		Fortnightly tiles		Preservation rates (%)	
	1	3	2	4	2 vs. 1	4 vs. 3
Cumulative thickness of couplets (mm)	303.2	335.4	65.0	92.2	21.4	27.5
Cumulative number of couplets	81	77	16	16	19.8	20.8
Average couplet thickness (mm)	3.7	4.4	4.1	5.8		
Sedimentation rate (cm year^{-1})	245.9	272.0	52.7	74.8		

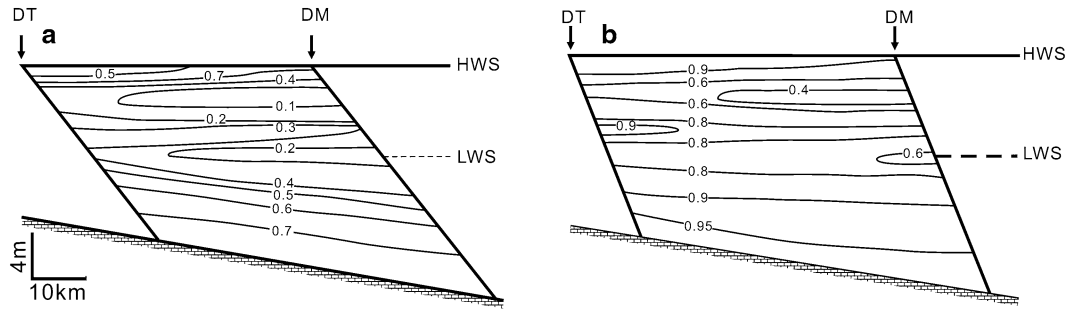

Fig. 9.30 Modeling output of the distribution pattern of the preservation potential over the transect DT-DM in Northern Jiangsu coast for different bed slopes: (**a**) tan $\beta = 0.5 \times 10^{-3}$; (**b**) tan $\beta = 1.0 \times 10^{-3}$ (After Gao 2009)

roughly 96 years, and were on average composed of 32 small successions (Fig. 9.31). The small succession is a storm-related thinning- and fining-upward succession, consisting of a couple of SDLs and MDLs, which are a group of sand- or mud-dominated layers, respectively, generated by storms or after the storms. Single small succession generally represents annual cycle of storm season and non-storm season deposition (Fig. 9.27), so only one third of 96-year depositional intervals contain their own deposits, and the diastems occupy the other two-third time intervals. Assuming the even distribution of the diastems, their temporal distribution is shown in Fig. 9.34a. Over 1-year interval, the temporal distribution of diastems looks like that of Fig. 9.34b, where the typhoon season and the following 1–2 months are marked in black with deposition of SDLs and MDLs. The latter can be deposited in a few weeks after the typhoon season on the basis of modern sedimentation rates, leaving the other several months blank or diastems during the non-typhoon season. Single SDLs can be formed by amalgamation of several storm deposits over a typhoon season as that shown in Fig. 9.27, and only the time intervals B, C, and D had the corresponding deposits preserved in the strata, leaving other time intervals blank (Fig. 9.27). The temporal distributions of diastems over the fortnightly and daily intervals were extrapolated from the tile observations. Meanly five to six sand-mud couplets on the fortnightly tiles and two sand-mud couplets on the daily tiles denote that 11 out of 14 days and 2 out of 4 semidiurnal tides were blank or without deposits over the fortnightly and daily intervals, respectively (Fig. 9.31c, d). It is therefore concluded that a sedimentary unit complete on a longer time scale actually contains many diastems on a shorter time scale. Diastems in the tidal-flat deposits can be generated by erosion of storm waves, and also by small waves and tides. They are discernible or non-discernible, representing the missing sediment intervals from a few hours to several years or longer (Fan et al. 2002).

9.7 Sedimentary Facies and Successions

9.7.1 Holocene Examples

9.7.1.1 Progradational Open-Coast Tidal-Flat Successions

The progradational open-coast tidal flats generally have a convex-up profile with marked fining-landward intertidal zonations. The regressive vertical stratigraphic

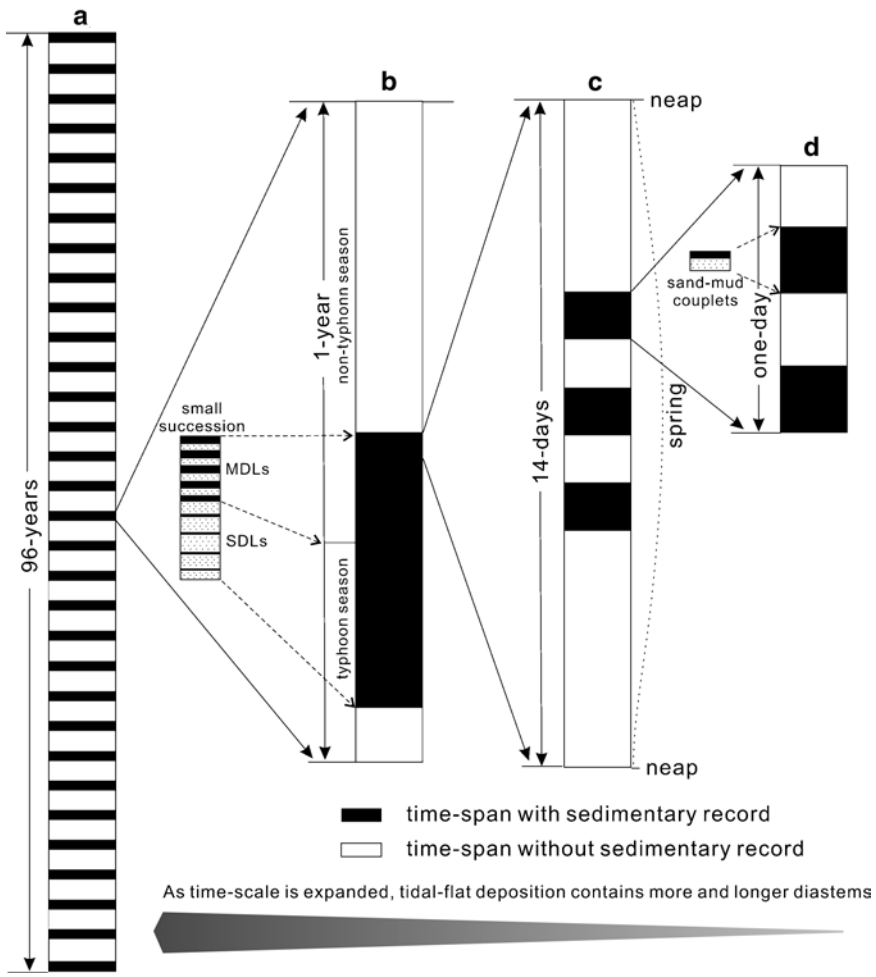

Fig. 9.31 The stratigraphic completeness of an open-coast intertidal-flat succession examined at different time scales, showing that a complete stratigraphic unit at a longer term was examined to fill with diastems at a shorter time scale. The intertidal-flat succession is roughly 4 m thick, deposited in ~96 years in the Changjiang Delta. The thickness of individual small successions and sand-mud couplets is generally a few centimeters to decimeters, and a few millimeters to centimeters (After Fan et al. 2002)

succession reflects this trend of variations, grading conformably upward from the lower intertidal sand, through the middle intertidal mud-sand mixture, to the upper intertidal mud (Fig. 9.32, Semeniuk 1981; Li and Li 1982; Li et al. 1992). The (shelly) sand facies generally consists of thick wave-rippled or massive sand layers with clay lenses or seams, and thick sand-dominated layers (SDLs, Fig. 9.26) of storm generation, developing cross-stratified bedding of slight bioturbation. The heterolithic mud and sand facies is characterized by abundant wavy bedding with moderate bioturbation and the small fining-upward successions consisting of alternative sand- and mud-dominated layers in roughly equal thickness. The mud facies grades upward from the upper bare to vegetated intertidal flats and usually continuing toward the supratidal flats, lithologically from finely laminated silt and clay with silty parallel to wavy laminae of a few grains to millimeters to massive mud with rippled sand lenses, scattered pigmentation mottles, and abundant in situ salt-marsh-plant rootlets or mangrove stumps. The laminated to bioturbated mottled mud may be interbedded with lensed beds of muddy and shelly sand of several decimeters thick or more, which are swash bar/chenier ridge deposits produced by storm waves (Semeniuk 1981; Li et al. 1992).

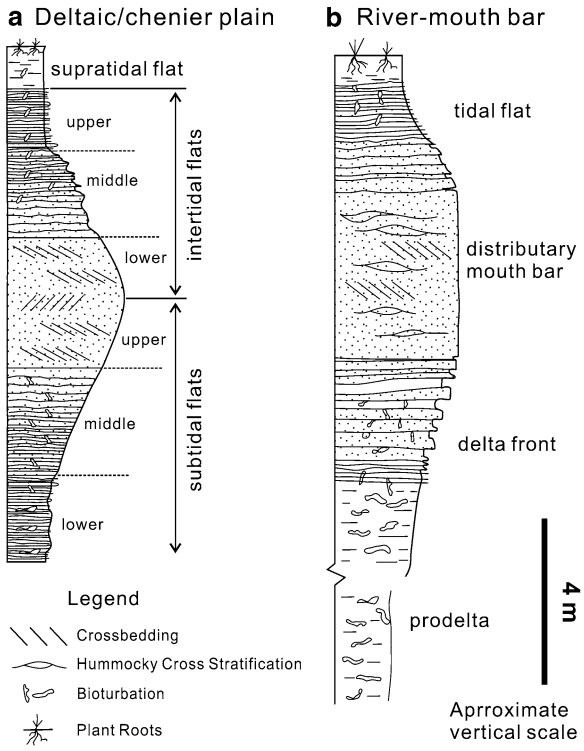

Fig. 9.32 Schematic models showing two most common progradational tidal-flat successions on the open-coast environment (After Li and Li 1982; Li et al. 1992; Dalrymple et al. 2003)

The progradational fining-upward intertidal-flat succession commonly continues with a coarsening-upward succession toward the subtidal flats for the muddy open-coast tidal flats with a gently smooth intertidal-subtidal profile (Fig. 9.32a, Li et al. 1992). It may also be underlain by the thick sand deposits when the muddy intertidal flats prograde over the subtidal sand-ridge systems like those on the central North Jiangsu coast (Ren 1985) and the distributary-mouth bars in the deltas (Fig. 9.32b; Dalrymple et al. 2003), or the sandy intertidal flats prograde over the subtidal ridge-runnel complex (Reineck and Cheng 1978; Semeniuk 1981).

9.7.1.2 Retrogradational Open-Coast Tidal-Flat Successions

The retrogradational sandy open-coast tidal flats commonly develop along the coast receiving slight sediment input, having a concave-up profile with general coarsening-landward trend of intertidal sediment distribution except the inner parts behind the swash bars/ridges (Yang et al. 2005, 2008a). They produce a transgressive coarsening-upward succession in response to Holocene sea-level rise (Fig. 9.33, Kim et al. 1999; Chang and Choi 2001; Lim et al. 2004; Yang et al. 2006b). The transgressive succession, usually unconformably underlain by either bedrock or pre-Holocene deposits which are commonly stiff mud (Kim et al. 1999), consists of three or four depositional units including the facies of salt-marsh, mud-, mixed-, and sand flats in an ascending order (units B_1–B_4 in Fig. 9.33). The lowermost unit (B_1), early Holocene salt-marsh deposit, is composed of intensively bioturbated dark-gray mud with minor sand-rippled lamination, rich in organic matter, and small plant roots. Unit B_2, mudflat deposit, is characterized by intensely bioturbated dark-gray mud with sporadic rhythmic lamination, grading conformably both downward and upward into units B_1 and B_3. Unit B_3, mixed-flat deposit, is composed of dark-gray, moderately bioturbated to laminated sandy silt or silty sand with relative abundance of shell fragments. The uppermost unit B_4, sand-flat deposit and unconformably overlying unit B_3, is characterized by greenish to olive gray, very fine to fine sand with slight bioturbation and relatively well-preserved lamination, typically developing storm-generated small fining-upward successions with hummocky cross-stratification (Fig. 9.28).

The whole Holocene coarsening-upward succession was previously interpreted as the result of the continual retrogradation of the non-barred tidal flats (Kim et al. 1999; Chang and Choi 2001; Lim et al. 2004), whereas the interpretation was questioned by Yang et al. (2006b). They noted that there was generally relative abundance of tidal creek/channel deposits (Fig. 9.33c) and absence of storm- or wave-generated structures in units B_1–B_3. These three units were consequently interpreted to be deposited in a back-barrier tidal-flat setting, because tidal channels are commonly rare on the modern open-coast tidal flats of the study area. As the transgression continued, the former barriers migrated landward over the back-barrier tidal flats, which thereafter changed into open-coast tidal flats (Fig. 9.33c). They become a wave-dominated setting with a volumetric majority of storm-generated beds (Yang et al. 2006b).

9.7.1.3 Estuarine-Deltaic Channel Filling Successions with Tidal Rhythms

A few examples have been reported to have the neap-spring cycles in recent and Holocene estuarine-deltaic channels, which lie between the truly open-coast and

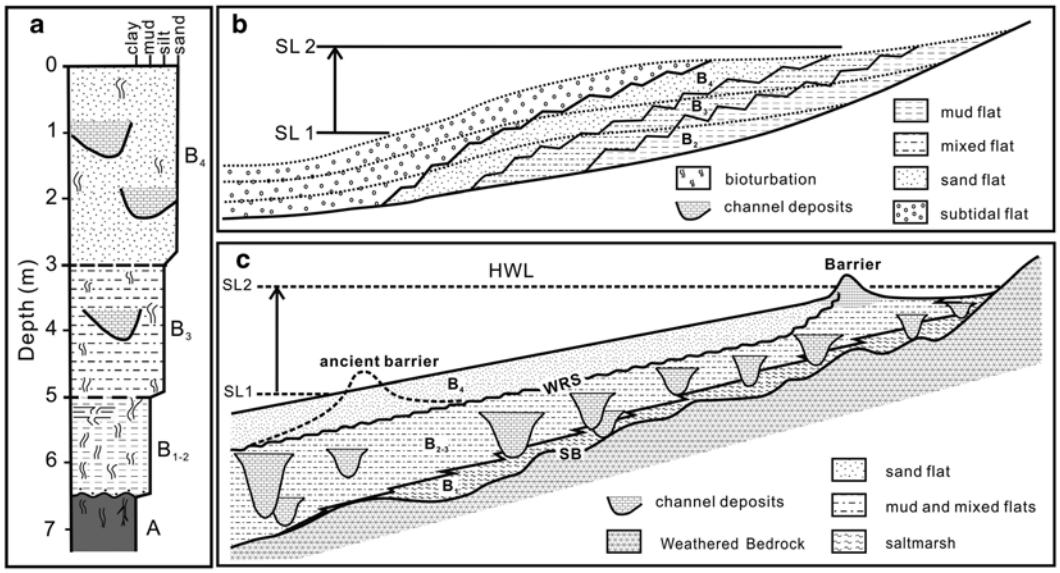

Fig. 9.33 (**a**) Schematic drawing of a retrogradational coarsening-upward tidal-flat succession, and (**b**, **c**) cross-shore profiles of vertical stacked tidal-flat sub-facies in response to sea-level rise on an open-coast setting with limited sediment input (After Kim et al. 1999; Yang et al. 2006b)

highly sheltered settings (Fan 2001; Hori et al. 2001; Dalrymple et al. 2003). In the Fly Delta, the recent vertical succession of tidal bar facies was found at a few core sections to exhibit cyclic changes in lithology. Each single cycle contains a lower half coarsening-upward succession and an upper half fining-upward succession, counting 26 sand laminae which are close to 28 tides for a semidiurnal tidal setting (Fig. 7a in Dalrymple et al. 2003). These features, together with the thick-thin alternation of adjacent sand laminae for the spring tidal deposits, have been undoubtedly interpreted to be the tide-generated neap-spring cycles and the diurnal inequality, respectively (Dalrymple et al. 2003).

Sand-mud couplets with cyclical changes in lamina thickness are common features in the early Holocene estuarine facies of the Changjiang Delta (Fan 2001; Hori et al. 2001). The core section of 47.12–48.49-m depth in the borehole CM-97 contains four complete neap-spring cycles (Fig. 9.34). The cycles are more clearly shown by variations in sand-laminae thickness (not including the very thin sand laminae within the mud couplets) through using 5-point adjacent averaging smoothing method. Discrete Fourier analysis of the smoothed data shows an average peak period at 28.4 laminae (25.2–31.5), matching well with 28 semidiurnal tides within a neap-spring cycle. Mud couplets and the superposition of current ripples with opposite foreset dipping directions are other good indicators of tidal origin. It is therefore hypothesized that the estuarine and deltaic-distributary channels potentially accommodate some rapid filling successions containing the neap-spring cycles.

9.7.2 Ancient Examples

Ancient tidalites have been extensively studied in the last three decades, typically those registering tidal cycle signals. Due to an excessive passion for periodic cycles, the dramatic growing publications are biased toward the cyclic tidal rhythmites with the neap-spring cycles. Noncyclic rhythmites have been greatly neglected even though they may contain the seasonal wave-climate cycles. Only a few ancient tidal rhythmites have been undoubtedly interpreted as the open-coast tidal-flat environments (Klein 1970; Fan et al. 2004b).

9.7.2.1 Tonglu (Late Ordovician)

Tonglu tidalites of the Late Ordovician age are well outcropped along a roadcut near Tonglu County, Zhejiang Province, east-central China (Fan et al. 2004b). They are the uppermost member subdivision

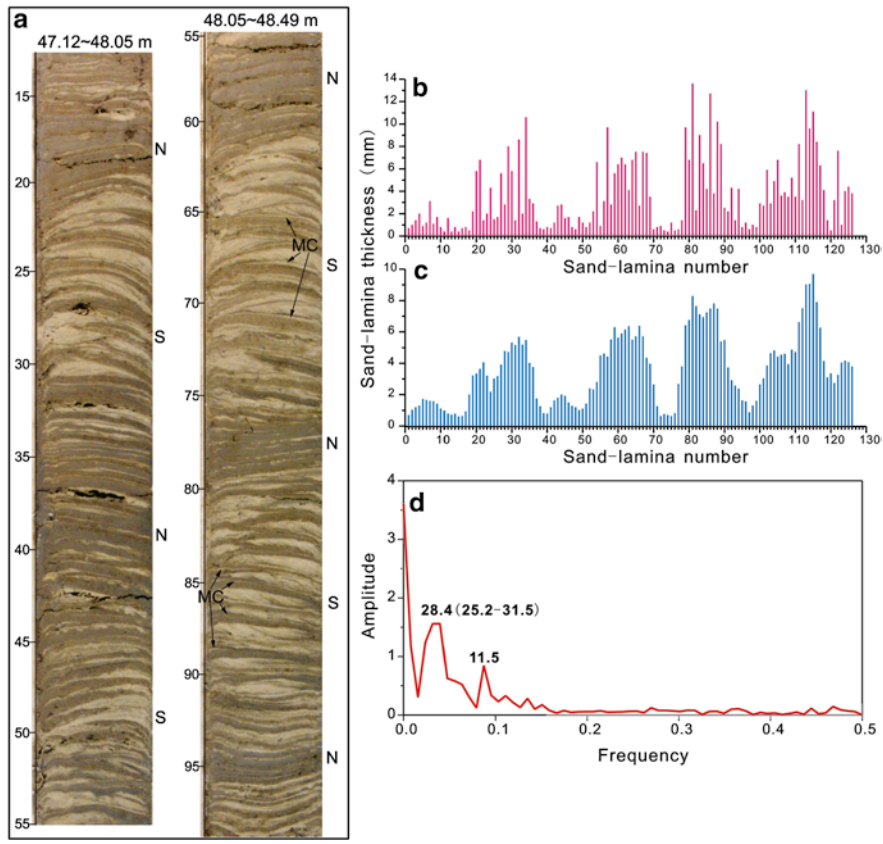

Fig. 9.34 Cyclic variations in sand-lamina thickness of the estuarine facies in the Changjiang Delta (depth of 47.12–48.49 cm along the borehole CM-97) deciphering neap-spring cycles. (**a**) Core photos; (**b** and **c**) plots of original data and smoothed data (using 5-point adjacent averaging method) of lamina thickness over lamina number; (**d**) FFT amplitude-frequency plot of the lamina-thickness data showing two major peak periods at 28.4 and 11.5 laminae. *N*, *S*, and *MC* in (**a**) are shortened for neap tide, spring tide, and mud couplets, respectively (After Fan 2001, photos courtesy of Yoshiki Saito)

of the Wenchang Formation, a shallowing-upward progradational succession from shallow marine to open coastal settings (Fig. 9.35). Tonglu tidalites exhibit three orders of periodicities in terms of sandstone and mudstone layer thickness. Millimeter- to centimeter-thick alternations of sandstone and mudstone laminae were ascribed to be deposited by single tidal cycles. Centimeter- to decimeter-thick alternations of sand-dominated layers (SDLs) and mud-dominated layers (MDLs) were interpreted to be formed by seasonal alternations of storm- and calm-wave climates. The storm-genesis interpretation of each single SDLs was convincingly based on the abundance of wave and storm action products, like intraformational mud pebbles, symmetrical wave ripples, and the asymmetrical small successions of thinning-upward trends which began with an erosion surface and overlain thick sandstone bed with abundant shell debris and mud pebbles, similar to modern storm-generated SDLs in the Changjiang Delta. The megacycle of several meters thick, composed of a lower half coarsening-upward succession and an upper half fining-upward succession, was interpreted as a vertical regressive succession produced by gradual shoaling from the lower subtidal zone to the upper intertidal zone with the coarsest and thickest sand layers at the middle, similar with that of modern open-coast tidal-flat depositional succession in Fig. 9.32a. Other evidence like general lack of tidal-channel filling deposits and abundance of wave-generated structures and small depositional successions also supports the open-coast tidal-flat environmental interpretation (Fan et al. 2004b).

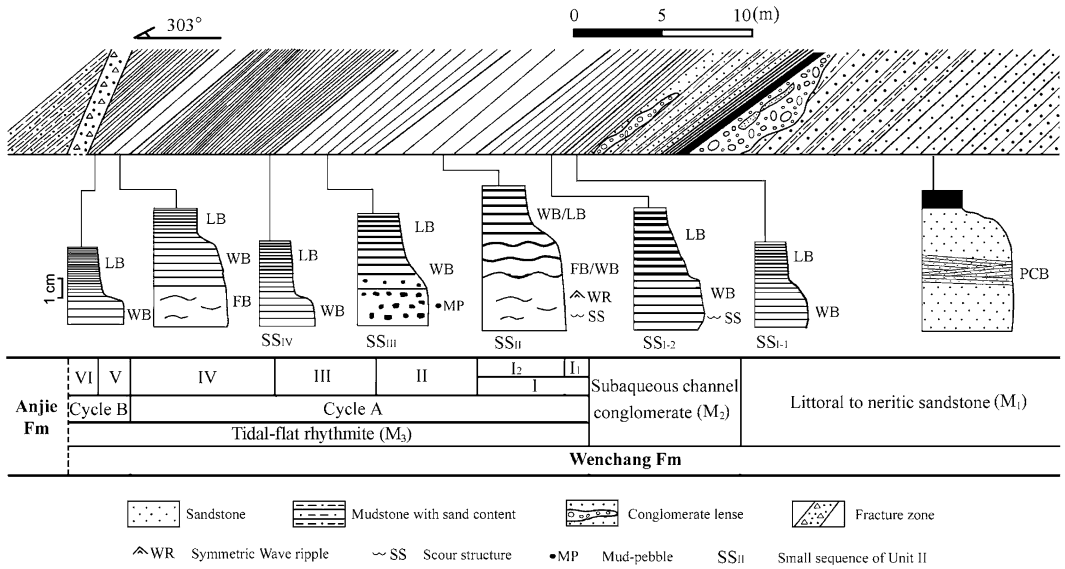

Fig. 9.35 Features of typical stratigraphic units compromising Tonglu tidal-flat successions, upper Wenchang Formation of Late Ordovician. The Tonglu tidal-flat successions consist of a complete cycle (A) from the subtidal facies to the upper intertidal facies and a half cycle (B) with upper part of intertidal facies associations. *PCB*, low-angle planar cross-bedding; *LB*, lenticular bedding; *WB*, wavy bedding; *FB*, flaser bedding; Anjie Fm, Anjie Formation of Early Silurian (After Fan et al. 2004b)

9.7.2.2 Islay (Late Proterozoic)

The Lower Fine-grained Quartzite of Middle Dalradian (Late Proterozoic) age in Islay, Scotland, consists of massive-bedded, cross-stratified, and rippled orthoquartzites (Facies 1), and siltstone and mudstone (Facies 2). The two facies are organized into a sharp-based, fining-upward succession with basal shallow subtidal sandstones, intertidal sand-flat or sand-bar sandstone, and high tidal-flat mudstones (Klein 1970). The succession is highly identical to that of back-barrier tidal-flat deposition (Klein 1985; Dalrymple 1992), except the general devoid of tidal-channel deposits. Comparison study prefers the modern analogue in the Wash of Eastern England with few presence of intertidal channels (Klein 1970), falling into the divisions of open-coast tidal flats.

9.7.2.3 Ramgundam (Middle Proterozoic)

The Ramgundam Sandstone of Middle Proterozoic age is well exposed along the Godavari Valley of south-central India (Chaudhuri and Howard 1985). It is composed of lens-shaped bodies of arkosic sandstone and interbedded sandstone and shale. The fining-upward succession devoid of tidal-channel deposits presumably represents a transgressive intertidal depositional succession building over linear-bar shoals frequently subjected to sufficient storm-induced wave activity (Chaudhuri and Howard 1985). Such facies interpretation sought no acceptable modern analogue at that time (Chaudhuri and Howard 1985), but is now comparable with the facies model of open-coast intertidal deposits building over the distributary-mouth or estuarine-channel bars (Fig. 9.32b).

9.7.2.4 Hazel Patch (Late Carboniferous)

The Hazel Patch sandstone of the Pennsylvanian age (Late Carboniferous) in eastern Kentucky (USA) has been highlighted for developing cyclic tidal rhythmites registering three orders of tidal cyclicities, including diurnal inequality, neap-spring cycle, and monthly tidal cycle (Greb and Archer 1995). Actually, cyclic tidal rhythmites are spatially limited in the lower part of a single major channel-filled succession. Within the channel fill, cyclic rhythmites grade upward into amalgamated rhythmites. The broad flats outside of the major channel are exclusively dominated by noncyclic rhythmites, containing small rhythmic successions similar to those of storm-generated successions on modern open-coast tidal flats (Figs. 9.27 and 9.28). The Hazel Patch sandstone is generally a fining-upward succession, consisting of the subtidal sand-bar deposits and the intertidal broad sand-flat deposits (both containing

extensive structures of combined-flow and storm genesis) and high intertidal-flat deposits containing numerous small tidal-channel fills (Greb and Archer 1995). The succession is also considered to be deposited on an open-coast intertidal flat over the distributary-mouth or estuarine-channel bars.

9.8 Summary

Tidal flats occupy a large section of the world's unsheltered shoreline, especially along the coast receiving large volumes of terrigenous fine sediments from rivers that build up broad and gentle shelf deposits. Open-coast tidal flats have received increasing interest because of their importance in global environmental issues posed by rising sea level, decreased sediment fluxes linking to river damming, and increasing human usage, also providing a modern analogue for fossil facies interpretation.

Large tidal range favors but is not a prerequisite for tidal-flat development. Sediment supply and the magnitude of wave exposure are two key controlling factors of tidal-flat morphology and sedimentology. Open-coast tidal flats develop in wide environments, ranging from partly exposed embayments and estuaries to highly exposed deltas and coastal plains. The commonest open-coast tidal flats are principally composed of mud, extensively distributing along the tide-dominated mega-deltas and their adjacent chenier plains. Most of the world's largest river deltas are tide dominated or under significant tidal influence. Littoral currents carry the resuspended sediment from the deltas, downdrift for tens to hundreds of kilometers along the coast to nourish tidal flats. The longest stretches of open-coast tidal flats are of this type, including the muddy coast along the East China and the Guianas. Sandy open-coast tidal flats majorly develop in the open-mouth estuaries and the adjacent strand plains, where large tidal ranges usually occur owing to tide amplification by typical coastal morphology, like narrow and shallow straits or funnel-shaped estuaries.

Open-coast tidal flats bare some common features to distinguish them from other coastal environments. These features include: (1) developing broad and gentle flats without significant morphological break along the shore-normal profile, (2) fronting an open sea or ocean without barriers, (3) exposing to different magnitudes of wave action with clear seasonal variations from tide-dominated into wave-dominated morphodynamic conditions, (4) developing few tidal channels on the bare flats except complex tidal-creek systems in the adjacent salt-marsh land, (5) exhibiting clear intertidal zonations of a coarsening seaward trend, and (6) containing abundant combined-flow and wave-induced structures and bedding.

It is noteworthy that there is a significant difference between the muddy and sandy open-coast tidal flats. The muddy classification tends to have an accretional convex-up profile with the coarsest sediment near the mean lower water springs, and develop a cyclic progradational succession consisting of a lower half of subtidal coarsening-upward succession and an upper half of a fining-upward intertidal-to-supratidal succession. The sandy type usually has an erosional concave-up profile with the coarsest sediment near the mean high water, and develops a coarsening-upward retrogradational succession. Typical hummocky cross-stratification (HCS) of short wavelength can be common in the sandy open-coast tidal-flat deposits, whereas not present in muddy open-coast tidal-flat deposits. The vertical succession of sandy open-coast tidal flats generally has higher abundance of storm-generated beds volumetrically than that of muddy open-coast tidal flats. A spectrum of coastal morphodynamic settings is therefore reorganized to change from the wave-influenced, tide-dominated muddy open-coast tidal flats, the wave- and tide-dominated accretional sandy open-coast tidal flats, wave-dominated erosional sandy open-coast tidal flats, to wave-dominated tidal beaches.

The open-coast tidal-flat deposition is far from complete (or continuous) due to reworking by complex physical processes. The well-developed sand-mud couplets do not represent the continuous deposition of tidal cycles in the vertical stacking succession. The preservation potential of strata is very low in terms of preservation rates of couplets and a general decreasing trend of sedimentation rates over different time scales. So the basic stratigraphic tenet is highlighted that deposition by shorter-time cyclic processes (e.g., tide) is highly reworked by successive longer-time cyclic processes (e.g., seasonal alternations of wave climate). Rapid continuous deposition with the neap-spring cycles is generally exempted from the open-coast tidal flats, except the relatively protected setting like the estuarine or distributary channels.

Following the recent research advances in open-coast tidal flats, the classification of clastic coastal environments should be changed to account for this new knowledge. New efforts should undoubtedly be steered to build new facies models for newly proposed subdivisions and to clarify the inter-relationships among any two transitional facies. Open-coast tidal flats are shaped by the interactions of tides and waves instead of their separate action, so the modulation of waves by tide should be stressed in the roles of sediment dynamics and morphodynamics. A renaissance is highly expected using integrative available data on both descriptive and quantitative features for ancient tidal facies interpretation after the three decades of research on tidal cycles. Muddy coasts adjacent to river deltas are undergoing great impacts (e.g., coastal erosion, wetland degradation) from human activities and global change, so modern environmental issues should be included and studied in the geological and sedimentologic aspects.

References

Alexander CR, Nittrouer CA, DeMaster DJ et al (1991) Macrotidal mudflats of west Korea: a model for interpretation of intertidal deposits. J Sediment Pet 61:805–824

Allen JRL, Duffy MJ (1998) Temporal and spatial depositional patterns in the Severn Estuary, SW Britain: intertidal studies at spring-neap and seasonal scales, 1991–1993. Mar Geol 146:147–171

Allison MA, Lee MT (2004) Sediment exchange between Amazon mudbanks and shore-fringing mangroves in French Guiana. Mar Geol 208:169–190

Allison MA, Nittrouer CA, Faria LEC (1995a) Shoreline morphology downdrift of the Amazon river mouth. Mar Geol 125:373–392

Allison MA, Nittrouer CA, Kineke GC (1995b) Seasonal sediment storage on mudflats adjacent to the Amazon River. Mar Geol 125:303–328

Allison MA, Lee MT, Ogston AS (2000) Origin of mud banks along the northeast coast of South America. Mar Geol 163:241–256

Amos C (1995) Siliclastic tidal flats. In: Perillo GME (ed) Geomorphology and sedimentology of estuaries, Advancement in Sedimentology 53. Elsevier, Amsterdam, pp 273–306

Anderson FE, Black L, Watling LE et al (1981) A temporal and spatial study of mudflat erosion and deposition. J Sediment Pet 51:729–736

Archer AW (1998) Hierarchy of controls on cyclic rhythmite deposition: Carboniferous basins of eastern and mid-continental, U.S.A. In: Alexander CR, Davis RA Jr, Henry VJ (eds) Tidalites: processes and products, SEPM Special Publications 61. SEPM, Tulsa, pp 59–68

Archer AW, Hubbard MS (2003) Highest tides of the world. In: Chan MA, Archer AW (eds) Extreme depositional environments: mega and members in geologic time, Geological Society of America Special Publication 370. Geological Society of America, Boulder, pp 151–173

Augustinus PGEF (2004) The influence of trade winds on the coastal development of the Guianas at various scale levels. Mar Geol 209:145–151

Baker EK, Harris PT, Keene JB et al (1995) Patterns of sedimentation in the macrotidal Fly River delta, Papua New Guinea. In: Flemming BW, Bartholoma A (eds) Tidal signatures in modern and ancient sediments, International Association of Sedimentology Special Publication 24. Elsevier, New York, pp 193–211

Baltzer F, Allison M, Fromard F (2004) Material exchange between the continental shelf and mangrove-fringed coasts with special reference to the Amazon-Guianas coast. Mar Geol 208:115–126

Boersma JR, Terwindt JHJ (1981) Neap-spring tide sequences of intertidal shoal deposits in a mesotidal estuary. Sedimentology 28:51–170

Boggs S Jr (2005) Principle of sedimentology and stratigraphy, 4th edn. Prentice Hall, New Jersey

Boguchwal LA, Southard JB (1990) Bed configurations in steady unidirectional water flows. Part 2. Synthesis of flume data. J Sediment Pet 60:658–679

Byrne JV, Jeroy DO, Riley CM (1959) The chenier plain and its stratigraphy, southwestern Louisiana. Trans Gulf Coast Assoc Geol Soc 9:237–260

Chang JH, Choi JY (2001) Tidal-flat sequence controlled by Holocene sea-level rise in Gomso Bay, west coast of Korea. Estuar Coast Shelf Sci 52:391–399

Chaudhuri A, Howard JD (1985) Ramgundam Sandstone: a Middle Proterozoic shoal-bar sequence. J Sediment Pet 55:392–397

Christie MC, Dyer KR, Turner P (1999) Sediment flux and bed level measurements from a macro tidal mudflat. Estuar Coast Shelf Sci 49:667–688

Coughenour CL, Archer AW, Lacovara KJ (2009) Tides, tidalites, and secular changes in the Earth-Moon system. Earth Sci Rev 97:59–79

Dalrymple RW (1992) Tidal depositional systems. In: Walker RG, James NP (eds) Facies models: response to sea level change, 2nd edn. Geological Association of Canada, St. John's, pp 195–218

Dalrymple RW (2010) Tidal depositional systems. In: James NP, Dalrymple RW (eds) Facies models 4, 2nd edn. Geological Association of Canada, St. John's, pp 195–218

Dalrymple RW, Makino Y, Zaitlin BA (1991) Temporal and spatial patterns of rhythmite deposition on mud flats in the macrotidal Cobequid Bay-Salmon River estuary, Bay of Fundy, Canada. In: Smith DG, Reinson GE, Zaitlin BA et al (eds) Clastic tidal sedimentology, Canadian Society of Petroleum Geologists Memoir 16. Canadian Society of Petroleum Geologists, Calgary, pp 137–160

Dalrymple RW, Baker EK, Harris PT et al (2003) Sedimentology and stratigraphy of a tide-dominated, foreland-basin delta (Fly River, Papua New Guinea). In: Sidi FH, Nummedal D, Imbert P et al (eds) Tropical deltas of southeast Asia-sedimentology, stratigraphy, and petroleum geology, SEPM Special Publication 76. SEPM, Tulsa, pp 147–173

Dalrymple RW, Yang BC, Chun SS (2006) Sedimentation on a wave-dominated, open-coast tidal flat, south-western Korea: summer tidal flat-winter shoreface – reply. Sedimentology 53:693–696

Davies JL (1972) Geographical variation in coastal development. Hafner Publishing, New York

Davis RA Jr, Hayes MO (1984) What is a wave-dominated coast? Mar Geol 60:313–329

Davis RA Jr, Alexander CR, Henry VJ (1998) Tidal sedimentology: historical background and current contributions. In: Alexander CR, Davis RA Jr, Henry VJ (eds) Tidalites: processes and products, SEPM Special Publication 61. SEPM, Tulsa, pp 1–4

Deloffre J, Verney R, Lafite R et al (2007) Sedimentation on intertidal mudflats in the lower part of macrotidal estuaries: sedimentation rhythms and their preservation. Mar Geol 241:19–32

ECCE (Editorial Committee for Chinese Embayments) (1992) Chinese embayments (Part V): Shanghai and North Zhejiang. China Ocean Press, Beijing (in Chinese)

Eisma D (1998) Intertidal deposits: river mouths, tidal flats, and coastal lagoons. CRC Press, New York

Eisma D, Augustinus PGEF, Alexander CA (1991) Recent and subrecent changes in the dispersal of Amazon mud. Neth J Sea Res 28:181–192

Fan DD (2001) Formation and preservation of rhythmic Deposition on the mudflats and quantitative analyses on diastems. PhD thesis, Tongji University, Shanghai (in Chinese with an English abstract)

Fan DD, Li CX (2002) Rhythmic deposition on mudflats in the mesotidal Changjiang estuary, China. J Sediment Res 72:543–551

Fan DD, Li CX, Chen MF et al (2001) Preservation potential of individual couplet and deposition rates on mudflats in the Changjiang Estuary. Sci China Ser B 44(supp):33–3

Fan DD, Li CX, Archer AW et al (2002) Temporal distribution of diastems in deposits of an open-coast intertidal flat with high suspended sediment concentrations. Sediment Geol 186:211–228

Fan DD, Li CX, Wang DJ et al (2004a) Morphology and sedimentation on open-coast intertidal flats of the Changjiang Delta, China. J Coast Res 43(Spec Issue):23–35

Fan DD, Li CX, Wang P (2004b) Influences of storm erosion and deposition on rhythmites of the Upper Wenchang Formation (Upper Ordovician) around Tonglu, Zhejiang Province, China. J Sediment Res 74:527–53

Fan DD, Guo YX, Li CX et al (2005) Grain-size distributions and their applications on Andong intertidal facies analyses in Hangzhou Bay. J Tongji Univ Nat Sci 33:687–691 (in Chinese with an English abstract)

Fan DD, Guo YX, Wang P (2006) Cross-shore variations in morphodynamic processes of an open-coast mudflat in the Changjiang Delta: with an emphasis on storm impacts. Cont Shelf Res 26:517–538

Frey RW, Howard JD, Han SJ et al (1989) Sediments and sedimentary sequences on a modern macrotidal flat, Inchon, Korea. J Sediment Petrol 59:28–44

Froidefond JM, Pujos M, Andre X (1988) Migration of mudbanks and changing coastline in French Guiana. Mar Geol 84:19–30

Gao S (2009) Modeling the preservation potential of tidal flat sedimentary records, Jiangsu coast, eastern China. Cont Shelf Res 29:1927–1936

Ginsburg RN (1975) Tidal deposits, a casebook of recent examples and fossil counterparts. Springer, Berlin

Greb SF, Archer AW (1995) Rhythmic sedimentation in a mixed tide and wave deposit, Hazel Patch sandstone (Pennsylvanian), eastern Kentucky coal field. J Sediment Res 65:96–106

Green MO, Black KP, Amos CL (1997) Control of estuarine sediment dynamics by interactions between currents and waves at several scales. Mar Geol 114:97–116

Hale PB, McCann SB (1982) Rhythmic topography in a mesotidal, low-wave-energy environment. J Sediment Pet 52:415–429

Harris PT, Baker EK, Cole AR et al (1993) A preliminary study of sedimentation in the tidally dominated Fly River Delta, Gulf of Papua. Cont Shelf Res 13:441–472

Hori K, Saito Y, Zhao QH et al (2001) Sedimentary facies of the tide-dominated paleo-Changjiang (Yangtze) estuary during the last transgression. Mar Geol 177:331–351

Huo M, Fan DD, Lu Q, et al (2010) Decadal variations in the erosion/deposition pattern of the Nanhui Mudbank and their mechanism in the Changjiang Delta. Acta Oceanologica Sinica 32(5):41–51

Kim BO (2003) Tidal modulation of storm waves on a macrotidal flat in the Yellow Sea. Estuar Coast Shelf Sci 57:411–420

Kim YH, Lee HJ, Chun SS et al (1999) Holocene transgressive stratigraphy of a macrotidal flat in the southeastern Yellow Sea: Gomso bay, Korea. J Sediment Res 69:328–337

Kineke JC, Sternberg RW, Trowbridge JH et al (1996) Fluid-mud processes on the Amazon continental shelf. Cont Shelf Res 16:667–696

Kirby R (2000) Practical implications of tidal flat shape. Cont Shelf Res 20:1061–1077

Klein GD (1970) Tidal origin of a Precambrian quartzite – the Lower Fine-grained Quartzite (Middle Dalradian) of Islay, Scotland. J Sediment Pet 40:973–985

Klein GD (1975) Epilogue-tidal sedimentation: some remaining problems. In: Ginsburg RN (ed) Tidal deposits. Springer, Heidelberg, pp 407–410

Klein GD (1985) Intertidal flats and intertidal sand bodies. In: Davis RA Jr (ed) Coastal sedimentary environments, 2nd edn. Springer, New York, pp 187–224

Klein GD (1998) Clastic tidalites – a partial retrospective view. In: Alexander CR, Davis RA Jr, Henry VJ (eds) Tidalites: processes & products, SEPM Special Publication 61. SEPM, Tulsa, pp 5–14

Kuehl SA, Nitrouer CA, DEMaster DJ (1988) Microfabric study of fine-grained sediments: observations from the Amazon subaqueous delta. J Sediment Pet 58:12–23

Kvale EP, Archer AW, Johnson HR (1989) Daily, monthly, and yearly tidal cycles within laminated siltstones of the Mansfield Formation (Pennsylvanian) of Indiana. Geology 17:365–368

Le Hir P, Roberts W, Cazaillet O et al (2000) Characterization of intertidal flat hydrodynamics. Cont Shelf Res 20:1433–1459

Lee HJ, Chun SS, Chang JH et al (1994) Landward migration of isolated shelly sand ridge (chenier) on the macrotidal flat of

Gomso Bay, west coast of Korea: controls of storms and typhoon. J Sediment Res 64:886–893
Lee SC, Mehta AJ, Members of ASCE (1997) Problems in characterizing dynamics of mud shore profiles. J Hydraul Eng 123:351–361
Lee HJ, Jo HR, Chu YS et al (2004) Sediment transport on macrotidal flats in Garolim Bay, west coast of Korea: significance of wind waves and asymmetry of tidal currents. Cont Shelf Res 24:821–832
Lees BG (1992) The development of a chenier sequence on the Victoria Delta, Joseph Bonaparte Gulf, northern Australia. Mar Geol 103:215–224
Lefebvre JP, Dolique F, Gratiot N (2004) Geomorphic evolution of a coastal mudflat under oceanic influences: an example from the dynamic shoreline of French Guiana. Mar Geol 209:191–205
Li J (1990) Sediment transport on the Nanhui mudflat in the Changjiang Estuary. Acta Oceanologica Sinica 12:74–82 (in Chinese with English abstract)
Li CX, Li P (1982) Sediments and sand bodies on the tidal flats. Oceanol Limnol Sinica 13(1):48–59 (in Chinese with English abstract)
Li CX, Yang X, Zhuang Z et al (1965) Formation and evolution of the intertidal mudflat. J Shangdong Oceanogr Coll 2:21–31 (in Chinese with English abstract)
Li CX, Han C, Wang P (1992) Depositional sequences and storm deposition on low-energy coast of China. Acta Sedimentol Sinica 10:119–127 (in Chinese with English abstract)
Li CX, Wang P, Fan DD et al (2000) Open-coast intertidal deposits and the preservation potential of individual lamina: a case study from East-central China. Sedimentology 47:1039–1051
Li CX, Wang P, Fan DD (2005a) Tidal flat, open ocean coasts. In: Schwartz ML (ed) Encyclopedia of coastal science. Springer, Heidelberg, pp 975–978
Li GX, Yang ZG, Liu Y et al (2005b) Studies on the genetic types of sub-sottom sedimentary facies in the east China seas. Chinese Science Press, Beijing
Lim DI, Choi J, Shin IH (2004) Late Quaternary sedimentation on a macrotidal mudflat deposit in Namyang Bay, west coast of Korea. J Coast Res 20:478–488
Liu CZ, Walker HJ (1989) Sedimentary characteristics of cheniers and the formation of the chenier plains of East China. J Coast Res 5:353–368
Mao ZC (1987) The role of wave action in scouring and siltation processes of Nanhui Eastern Flats. Trans Oceanol Limnol 4:21–29
Meade RH, Dunne T, Richey JE et al (1985) Storage and remobilization of suspended sediment in the lower Amazon River of Brazil. Science 228:488–490
Meckel LD (1975) Holocene sand bodies in the Colorado Delta area, Northern Gulf of California. In: Broussard ML (ed) Deltas-models for exploration. Houston, Houston Geological Society, pp 239–265
Middleton GV (1991) A short historical review of clastic tidal sedimentology. In: Smith DG, Reinson GE, Zaitlin BA et al (eds) Clastic tidal sedimentology, Canadian Society of Petroleum Geologists Memoir 16. Canadian Society of Petroleum Geologists, Calgary, pp ix–xv
Milliman JD, Meade RH (1983) World-wide delivery of river sediment to the oceans. J Geol 91:1–21
Milliman JD, Syvitski JPM (1992) Geomorphic/tectonic control of sediment discharge to the ocean: the importance of small mountainous rivers. J Geol 100:525–544
Mukherjee KK, Das S, Chakrabarti AA (1987) Common physical sedimentary structure in a beach-related open-sea siliciclastic tropical tidal flat at Chandipur, Orissa, India and evaluation of the weather conditions through discriminant analysis. Senckenberg Marit 19:261–293
Nio SD, Yang CS (1991) Diagnostic attributes of clastic tidal deposits: a review. In: Smith DG, Reinson GE, Zaitlin BA, Rahmani RA (eds) Clastic tidal sedimentology, Canadian Society of Petroleum Geologists Memoir 16. Canadian Society of Petroleum Geologists, Calgary, pp 3–28
O'Brien DJ, Whitehouse RJS, Cramp A (2000) The cyclic development of a macrotidal mudflat on varying timescales. Cont Shelf Res 20:1593–1619
Park YA, Wells JT, Kim BW et al (1995) Tidal lamination and facies development in the macrotidal flats of Namyang Bay, west coast of Korea. In: Flemming BW, Bartholoma A (eds) Tidal signatures in modern and ancient sediments, International Association of Sedimentation Special Publication 24. Blackwell, Berlin, pp 183–191
Plaziat C, Augustinus PGEF (2004) Evolution of progradation/erosion along the French Guiana mangrove coast: a comparison of mapped shorelines since the 18th century with Holocene data. Mar Geol 209:127–143
Reineck HE, Cheng YM (1978) Sedimentology and faunistics of tidal flats in Taiwan. I. Marine geology. Senckenberg Marit 10:85–115
Reineck HE, Singh IB (1980) Depositional sedimentary environments, 2nd edn. Springer, Berlin
Ren ME (1985) Modern sedimentation in coastal and nearshore zone of China. Springer, Berlin
Rhodes EG (1982) Depositional model for a chenier plain, Gulf of Carpentaria, Australia. Sedimentology 29:201–222
Rine JM, Ginsburg RN (1985) Depositional facies of a mud shoreface in Suriname, South America – a mud analogue to study, shallow-marine deposits. J Sediment Pet 55:633–652
Ryu JH, Kim CH, Lee YK et al (2008) Detecting the intertidal morphologic change using satellite data. Estuar Coast Shelf Sci 78:623–632
Semeniuk V (1981) Long-term erosion of the tidal flats King Sound, northwestern Australia. Mar Geol 43:21–48
Shi Z, Chen JY (1996) Morphodynamics and sediment dynamics on intertidal mudflats in China (1961–1994). Cont Shelf Res 16:1909–1926
Talke SA, Stacey MT (2008) Suspended sediment fluxes at an intertidal flat: the shifting influence of wave, wind, tidal and freshwater forcing. Cont Shelf Res 28:710–725
Tessier B (1993) Upper intertidal rhythmites in the Mont-Saint-Michel Bay (NW France): perspectives for paleoreconstruction. Mar Geol 110:355–367
Thomas S, Ridd PV (2004) Review of methods to measure short time scale sediment accumulation. Mar Geol 207:95–114
Thompson RW (1968) Tidal flat sedimentation on the Colorado River delta, northwestern Gulf of California. Geol Soc Am Mem 107:413 p
Thompson RW (1975) Tidal-flat sediment of the Colorado River delta, northwestern Gulf of California. In: Ginsburg RN (ed) Tidal deposits: a casebook of recent examples and fossil counterparts. Springer, Heidelberg, pp 57–65

Walsh JP, Nittrouer CA (2004) Mangrove-bank sedimentation in a mesotidal environment with large sediment supply, Gulf of Papua. Mar Geol 208:225–248

Wang Y (1963) The coastal dynamic geomorphology of the northern Bohai Bay. In: Wang Y (ed) Collected oceanic works of Nanjing University. Nanjing University Press, Nanjing, pp 25–35 (in Chinese with English abstract)

Wang Y (1983) The mudflat system of China. In: Gordon DC Jr, Hourston AS (eds) Proceedings of the symposium on the dynamics of turbid coastal environments, Canadian Journal of Fish Aquatic Science 40. Government of Canada, Fisheries and Oceans, Ottawa, pp 160–171

Wang BC, Eisma D (1988) Mudflat deposition along the Wenzhou coastal plain in southern Zhejiang, China. In: DE Boer PL, VAN Gelder A, Nio SD (eds) Tide-influenced sedimentary environments and facies. D. Reidel Publishing Company, Dordrecht, pp 265–274

Wang BC, Eisma D (1990) Supply and deposition of sediment along the north bank of Hangzhou Bay, China. Neth J Sea Res 25:377–390

Wang Y, Ke SK (1989) Cheniers on the east coastal plain of China. Mar Geol 90:321–335

Wang XY, Ke XK (1997) Grain-size characteristics of the extant tidal flat sediments along the Jiangsu coast, China. Sediment Geol 112:105–122

Wang Y, Zhu DK, Wu XG (2002) Tidal flats and associated muddy coast of China. In: Healy T, Wang Y, Healy JA (eds) Muddy coasts of the world: processes, deposits and function. Elsevier, Amsterdam, pp 319–346

Wang AJ, Gao S, Chen J et al (2009) Sediment dynamic response of coastal salt marsh to typhoon "Kaemi" in Quanzhou Bay, Fujian Province, China. China Sci Bull 53:120–130

Wells JT, Coleman JM (1978) Longshore transport of mud by waves: northeastern coast of South America. Geol Mijn 57:353–359

Wells JT, Coleman JM (1981) Physical processes and fine-grained sediment dynamics, coast of Surinam, South America. J Sediment Pet 51:1053–1063

Wells JT, Adams CE Jr, Park YA et al (1990) Morphology, sedimentology and tidal channel processes on a high-tide-range mudflat, west coast of South Korea. Mar Geol 95:111–130

Williams GE (1997) Precambrian length of day and the validity of tidal rhythmite paleotidal values. Geophys Res Lett 24:421–424

Yang BC, Dalrymple RW, Chun SS (2005) Sedimentation on a wave-dominated, open-coast tidal flat, southwestern Korea: summer tidal flat – winter shoreface. Sedimentology 52:235–252

Yang BC, Dalrymple RW, Chun SS (2006a) The significance of hummocky cross- stratification (HCS) wavelengths: evidence from an open-coast tidal flat, south Korea. J Sediment Res 76:2–8

Yang BC, Dalrymple RW, Chun SS et al (2006b) Transgressive sedimentation and stratigraphic evolution of a wave-dominated macrotidal coast, western Korea. Mar Geol 235:35–48

Yang BC, Dalrymple RW, Chun SS et al (2008a) Tidally modulated storm sedimentation on open-coast tidal flats, southwestern coast of Korea: distinguishing tidal-flat from shoreface storm deposits. In: Hampson GJ, Steel RJ, Burgess PM, Dalrymple RW (eds) Recent advances in models of Siliciclastic shallow-marine stratigraphy, SEPM Special Publication 90. SEPM, Tulsa, pp 161–176

Yang BC, Gingras MK, Pemberton SG et al (2008b) Wave-generated tidal bundles as indicator of wave-dominated tidal flats. Geology 36:39–42

Yang SL, Li H, Ysebaert T et al (2008c) Spatial and temporal variations in sediment grain size in tidal wetlands, Yangtze Delta: on the role of physical and biotic controls. Estuar Coast Shelf Sci 77:656–671

Zhang RS, Wang XY (1991) Tidal creek system on tidal mud flat of Jiangsu Province. Acta Geog Sinica 46:195–206 (in Chinese with English abstract)